Dissipation Reduction and Information-to-Measurement Conversion in DNA Pulling Experiments with Feedback Protocols

M. Rico-Pasto,[1,†] R. K. Schmitt,[2,†] M. Ribezzi-Crivellari,[3] J. M. R. Parrondo,[4] H. Linke,[2] J. Johansson,[2] and F. Ritort[1,*]

[1]*Condensed Matter Physics Department, University of Barcelona, C/Marti i Franques 1, 08028 Barcelona, Spain*
[2]*Solid State Physics and NanoLund, Lund University, P.O. Box 118, SE-221 00 Lund, Sweden*
[3]*École Supérieure de Physique et de Chimie Industrielles-ESPCI Laboratoire de Biochimie (LBC), 75005 Paris, France*
[4]*Departamento de Estructura de la Materia, Física Térmica y Electrónica and GSIC, Universidad Complutense de Madrid, 28040 Madrid, Spain*

(Received 6 November 2020; revised 17 June 2021; accepted 30 June 2021; published 8 September 2021)

Information-to-energy conversion with feedback measurement stands as one of the most intriguing aspects of the thermodynamics of information in the nanoscale. To date, experiments have focused on feedback protocols for work extraction. Here we address the novel case of dissipation reduction in nonequilibrium systems with feedback. We perform pulling experiments on DNA hairpins with optical tweezers, with a general feedback protocol based on multiple measurements that includes either discrete-time or continuous-time feedback. While feedback can reduce dissipation, it remains unanswered whether it also improves free-energy determination (information-to-measurement conversion). We define thermodynamic information Υ as the natural logarithm of the feedback efficacy, a quantitative measure of the efficiency of information-to-energy and information-to-measurement conversion in feedback protocols. We find that discrete- and continuous-time feedback reduces dissipation by roughly $k_BT\Upsilon$ without improvement in free-energy determination. Remarkably, a feedback strategy (defined as a correlated sequence of feedback protocols) further reduces dissipation, enhancing information-to-measurement efficiency. Our study underlines the role of temporal correlations to develop feedback strategies for efficient information-to-measurement conversion in small systems.

DOI: 10.1103/PhysRevX.11.031052 Subject Areas: Biological Physics, Statistical Physics

I. INTRODUCTION

Maxwell's demon (MD) thought experiment [1] has led to the insight that information enhances the capacity to extract energy from a system. In 1961, Landauer demonstrated that any irreversible logical operation (such as bit erasure) dissipates at least $k_BT\log 2$ per stored bit of information [2]. Bennett [3] applied this result to the Szilards engine [1], a single-particle version of the MD that extracts energy from a thermal bath in a cycle. It was shown that bit erasure is an entropy-producing step necessary to restore the initial *blank* state of the memory of the demon, in agreement with the second law [4–6]. These developments have boosted a new field of research, namely, the thermodynamics of small systems under feedback control [7–10]. This has led to experimental realizations of the Maxwell demon in colloidal systems [11–14], electronic [15,16] and optical devices [17–19], single molecules [20], quantum systems [21–23], and tests of the Landauer limit [24–28]. The extension of stochastic thermodynamics [29–31] to include information and feedback has led to novel fluctuation theorems (FTs) for work and information [32–35], in repeated-time feedback protocols [36–39] and analytically solvable models [40–43]. Generalized Jarzynski equalities have been derived for isothermal feedback processes, where an external agent performs a single measurement on a system and applies a protocol ω_m that depends on the measurement outcome $m = 1, 2, \ldots, M$. A main equality useful for measurements with feedback reads [33]

$$\langle \exp\left[-(W-\Delta G)/k_BT\right]\rangle = \sum_{m=1}^{M} P_{\leftarrow}(m|\omega_m) \equiv \gamma \qquad (1)$$

*Corresponding author.
ritort@ub.edu
†Equally contributed authors.

with k_B the Boltzmann constant and T the temperature. Here, W is the work performed on the thermodynamic system, ΔG is the free-energy difference, and $P_{\leftarrow}(m|\omega_m)$ is the probability to measure m along the time reversal ($\leftarrow$) of the original protocol ω_m. Equation (1) defines the efficacy parameter $\gamma(\leq M)$ which quantifies the reversibility of the feedback process [44], reaching its maximum value (M) for reversible feedback process where $P_{\leftarrow}(m|\omega_m) = 1$ for all m. Without feedback, $\omega_m \equiv \omega$ and $\gamma = 1$, with Eq. (1) the Jarzynski equality. It is convenient to define the logarithm of the efficacy $\Upsilon = \log\gamma$, which is a bound of the work that can be extracted in an isothermal feedback process. Υ might be called thermodynamic information, information utilization, or negentropy. For discrete-time single measurements, Υ is bounded from above [Eq. (1)with $P_{\leftarrow}(m|\omega_m) \leq 1$], $-\infty < \Upsilon \leq \log M$ ($M = 2$ being the one-bit Landauer limit). Jensen's inequality applied to Eq. (1) yields

$$\langle W_d\rangle \equiv \langle W\rangle - \Delta G \geq -k_BT\Upsilon \Rightarrow \langle W_d\rangle + k_BT\Upsilon \geq 0, \quad (2)$$

where $\langle W_d\rangle$ is the dissipated work. Without feedback, $\Upsilon = 0$ and $\langle W_d\rangle_0 \geq 0$ where the subscript 0 denotes the nonfeedback case. In experimental realizations of the MD, feedback measurement is operated in equilibrium systems and $\Upsilon = \log M$ is the maximum extractable (i.e., negative) work for equally likely outcomes, $\langle W\rangle = -k_BT\Upsilon = -k_BT\log M$.

Here we address a novel situation where feedback is operated to reduce dissipation in small nonequilibrium systems. Most systems in nature and daily life applications are out of equilibrium and dissipative, requiring feedback to reduce dissipation. Examples range from heat engines that minimize heat dissipation to control energy production and avoid extreme events (e.g., accidents in power plants) to living organisms. Most regulatory processes in the cell focus on housekeeping tasks: The entropy production must be kept within bounds and reduced upon unexpected rises due to exogenous (external) factors. The understanding of dissipation reduction is vital in the nanoscale where dissipative molecular processes are remarkably efficient (for instance, the typical >90% efficiency of the Adenosine triphosphate enzymes [ATPase] machinery). In all these nonequilibrium systems, dissipation reduction by using feedback is critical. The main goal of this paper is to derive and test fluctuation theorems describing dissipation reduction in such kinds of systems.

For a nonequilibrium process, Eq. (2) shows that dissipation is bounded by $-k_BT\Upsilon$. For $\Upsilon > 0$ (information-to-work conversion), dissipation is reduced by at most $-k_BT\Upsilon$. Conversely, one could apply feedback protocols where $\Upsilon < 0$ (information-to-heat conversion) and dissipation increases by at least $-k_BT\Upsilon$. The latter case is nonproductive feedback for dissipation reduction. It has similarities to feedback in control theory, where protocols regulate experimental variables, e.g., by keeping them constant [45,46]. These types of protocols counteract deviations from a system's specific preset conditions rather than rectifying thermal fluctuations, leading to increased dissipation. For the relevant case $\Upsilon > 0$, the dissipated work is reduced with respect to the nonfeedback case $\langle W_d\rangle \leq \langle W_d\rangle_0$. We define the information-to-energy or feedback-cycle efficiency [47–49] η_I as the reduction in dissipation $\Delta\langle W_d\rangle = \langle W_d\rangle_0 - \langle W_d\rangle$ relative to the second law bound $\langle W_d\rangle_0 + k_BT\Upsilon$:

$$\eta_I = \frac{\Delta\langle W_d\rangle}{\langle W_d\rangle_0 + k_BT\Upsilon} < 1. \quad (3)$$

This is our first key result for information-to-work conversion in nonequilibrium conditions. For cyclic and reversible MD devices $\langle W_d\rangle_0 = 0$, so $\eta_I = -\langle W_d\rangle/k_BT\Upsilon$ is the standard MD efficiency.

Related to dissipation reduction is free-energy determination, a relevant question for molecular thermodynamics where important applications have emerged in molecular folding and ligand binding [50–52]. It is an open question whether, by reducing dissipation, feedback can improve free-energy determination, what we call information-to-measurement conversion. Free-energy determination can be improved if $\langle W_d\rangle + k_BT\Upsilon < \langle W_d\rangle_0$, which we denote as weakening of the second law. Free-energy determination improvement is related to the Jarzynski relation Eq. (1) and its bias B_N for N work (W) measurements. Inserting $\Upsilon = \log\gamma$ into Eq. (1), we define

$$\begin{aligned} B_N &= \langle \Delta G_N\rangle - \Delta G, \\ \Delta G_N &= -k_BT\log\left(\frac{1}{N}\sum_{i=1}^{N} e^{-\frac{W_i}{k_BT}}\right) + k_BT\Upsilon \end{aligned} \quad (4)$$

with ΔG_N the Jarzynski ΔG estimator for N experiments and $\langle..\rangle$ the average over many realizations of the N experiments. The exponential average of minus the work in Eq. (4) is biased for finite N [whereas the bounded and finite sum defining $\Upsilon(=\log\gamma)$ in Eq. (1) is not]. B_N is positive and monotonically decreasing with N [53], vanishing in the limit $N \to \infty$. Therefore, improved free-energy determination requires that B_N for $N = 1$ decreases with feedback relative to the nonfeedback case. From Eq. (4) we have

$$\begin{aligned} B_1 &= \langle \Delta G_1\rangle - \Delta G = \langle W\rangle - \Delta G + k_BT\Upsilon \\ &= \langle W_d\rangle + k_BT\Upsilon \geq 0, \end{aligned} \quad (5)$$

which is equivalent to Eq. (2). Therefore, weakening of the second law implies reducing B_1, leading to improved free-energy determination for finite N.

To quantify information-to-measurement conversion, we define the cycle efficiency η_M as the relative difference

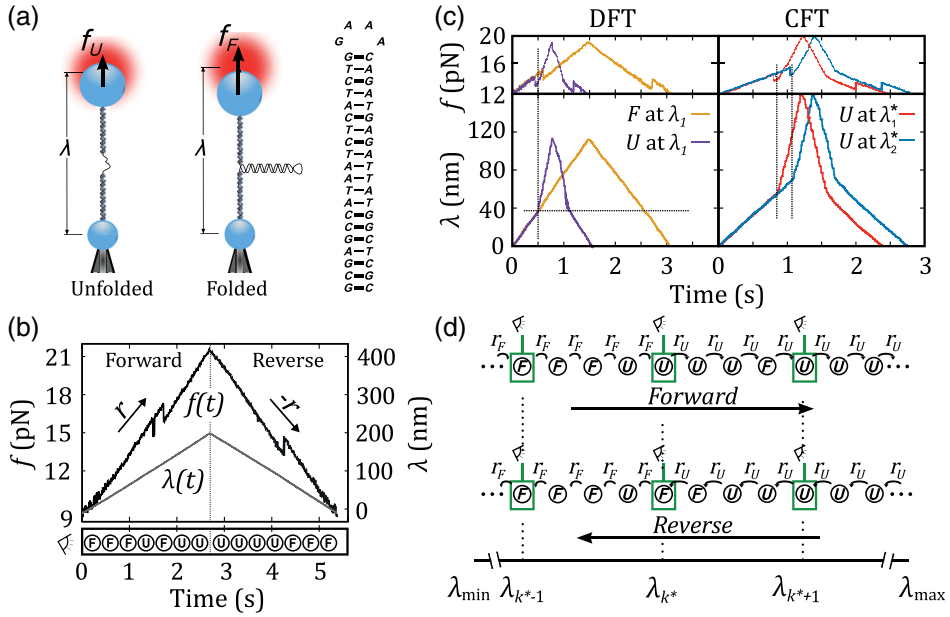

FIG. 1. DNA pulling experiments with feedback measurement. (a) Schematics of the single-molecule experimental setup. The optical trap measures the force f applied on the molecule. The control parameter λ denotes the distance between the optical trap and the pipette. The DNA hairpin sequence is shown on the right. (b) Experimental unfolding and refolding FDCs without feedback, where we plot both f and λ as a function of time. λ (color gray, scale on the right side) is first increased (unfolding and forward process) at a constant loading rate $r = 4$ pN/s. After reaching a predefined upper value, λ is decreased at the unloading rate r (folding and reverse process). Along the time axis, we show the sequence of states (F, folded; U, unfolded) observed at specific times along the trajectory (note the transient refolding event along $\rightarrow$). (c) Left: pulling protocol with DTF. The initial pulling rate r_F is switched to r_U (purple) if the molecule is found to be unfolded (U) at λ_1 and is unchanged otherwise (orange). Right: pulling protocol with CTF. The pulling rate r_F along $\rightarrow$ is switched to r_U as soon as an unfolding event is detected. In both cases, the protocol in the $\leftarrow$ process is the time reversal of the one used in the $\rightarrow$ process. (d) Schematics of the general first-time-feedback (FTF) protocol in a pulling experiment. The state of the system (F or U) is repeatedly observed during $\rightarrow$ at specified values of the control parameter λ_k (green boxes). At λ_{k^*}, the system is observed to be in U for the first time, and the pulling rate is switched from r_F to r_U. In the illustration, the first time the molecule is found to be in U along the predetermined set of λ_k occurs at λ_{k^*}: The molecule was in F at all observed trap positions before λ_{k^*} (with λ_{k^*-1} the previous trap position where F was observed). Note that the molecule can execute multiple transitions at intermediate values of λ (between λ_{k^*-1} and λ_{k^*}) where no observations are made. A feedback response is triggered only when state U is observed for the first time at the specific positions defined by the predetermined set $\{\lambda_k\}$.

between the second law inequality bounds with feedback $\langle W_d\rangle + k_BT\Upsilon \geq 0$ and without feedback $\langle W_d\rangle_0 \geq 0$:

$$\eta_M = 1 - \frac{\langle W_d\rangle + k_BT\Upsilon}{\langle W_d\rangle_0} = \eta_I + (\eta_I - 1)\frac{k_BT\Upsilon}{\langle W_d\rangle_0}. \quad (6)$$

This is our second main result, which leads to a new inequality $\eta_M \leq \eta_I$. Note that $\eta_M = 1$ if and only if $\eta_I = 1$, in which case dissipation reduction is maximal $\langle W_d\rangle = -k_BT\Upsilon$, and $\Delta G = \langle W\rangle + k_BT\Upsilon$ can be determined with certainty. Improved free-energy determination requires $\eta_M > 0$, whereas for $\eta_M \leq 0$, no gain in free-energy determination is obtained with feedback: $\langle W_d\rangle$ decreases with respect to $\langle W_d\rangle_0$ by exactly or less than $k_BT\Upsilon$. In general, optimal free-energy determination is obtained by maximizing η_M.

Here we address information-to-energy and information-to-measurement conversion by combining theory and experiment. We introduce a new feedback FT for multiple repeated measurements that is applicable to DNA unzipping experiments with optical tweezers [Fig. 1(a) and Sec. II A]. From the pulling experiments, we measure the work distributions and Υ to extract the efficiencies η_I, η_M. We investigate whether reduced dissipation with feedback ($\Upsilon > 0$) improves free-energy determination. In a pulling experiment without feedback, the optical trap is repeatedly ramped up (forward, $\rightarrow$) and down (reverse, $\leftarrow$) at a constant speed between trap positions $\lambda_{\min}$ and $\lambda_{\max}$ where the molecule is folded (F) and unfolded (U), respectively, while the force f exerted by the trap is measured, producing a force-distance curve (FDC) [Fig. 1(b) and Sec. II B]. We apply two different feedback protocols, namely, discrete-time feedback (DTF) [Fig. 1(c), left] and continuous-time feedback (CTF) [Fig. 1(c), right]. The CTF protocol is the nonequilibrium generalization of a recently introduced continuous Maxwell demon [20], DTF and CTF being particular cases of the new feedback protocol. We show that, while DTF and CTF protocols

mildly reduce dissipation, they do not improve free-energy determination ($\eta_M \lesssim 0$). Remarkably, a feedback strategy combining DTF and CTF protocols markedly increases η_I and η_M. This sets feedback strategies (defined as a sequence of multiple-correlated feedback protocols) as the route to enhance the nonequilibrium information-to-energy and -measurement efficiencies.

II. MATERIALS AND METHODS

A. Instrument design and single-molecule construct

The instrument used in this study is a miniaturized optical tweezers setup [54] with counterpropagating lasers focused into the same point to create a single optical trap. The control parameter for the device is the position of the optical trap with respect a fixed point, in our case the bead immobilized on the tip of a micropipette [Fig. 1(a)]. Force is directly measured from the change in light momentum of the deflected beam using position-sensitive detectors. The molecular construct is manipulated by using two polystyrene beads, one coated with antidigoxigenin, the other with streptavidin, that are connected to opposite ends of the molecular construct through antigen-antibody and biotin-streptavidin bonds, respectively.

For the experiments, we use a molecular construct made of a short DNA hairpin linked to molecular handles on both flanking sides. The DNA hairpin has a stem consisting of 20 base pairs (bp) and a tetraloop (underlined), (5'-GCGAGCCATAATCTCATCTG GAAA CAGATGAGATTATGGCTCGC-3') that unfolds and refolds cooperatively in a two-state manner. It is flanked by two identical 29 bp double-stranded DNA handles [55]. The molecular handle is tagged with a single biotin at the 3'-end, while the other end is tagged with multiple digoxigenins. For pulling experiments, the molecular construct (DNA hairpin plus handles) is tethered between two beads, one is captured in the optical trap and the other is immobilized on the tip of a glass micropipette.

B. Pulling experiments and work measurements

In pulling experiments without feedback, a mechanical force is applied to the ends of the molecular construct [Fig. 1(a)]. At low forces, typically below 10 pN, the hairpin remains in its native double-stranded configuration (folded state, F), while at higher forces it unfolds to its single-stranded DNA configuration (unfolded state, U). Every pulling cycle consists of two processes [Fig. 1(b)]: the forward (unfolding) process ($\rightarrow$) where the molecule is initially in F at $\lambda_{\rm min}$ and the force f increases at a constant loading rate r until $\lambda_{\rm max}$ is reached. During this process, the molecule unfolds, entering state U, and the force drops by $\Delta f \sim 1$ pN. In the reverse (folding) process ($\leftarrow$), the molecule is initially in U at $\lambda_{\rm max}$ and the force is decreased at the unloading rate $-r$ until reaching $\lambda_{\rm min}$. When the molecule folds, the force rises by the same amount $\Delta f \sim 1$ pN. For a given trajectory, one can extract the work W exerted by the optical trap on the molecular construct. W is defined as the area below the force-distance curve $W_{\rightarrow(\leftarrow)} = +(-)\int_{\lambda_{\rm min}}^{\lambda_{\rm max}} f d\lambda$ with positive (negative) W values for the $\rightarrow$ ($\leftarrow$) process. The pulling experiment defines a thermodynamic transformation on the molecular system (DNA hairpin, handles, and bead) between trap positions $\lambda_{\rm min}$ and $\lambda_{\rm max}$ with free-energy difference $\Delta G_{\rm FU} = G_U(\lambda_{\rm max}) - G_F(\lambda_{\rm min})$. The second law states that $\langle W\rangle_{\rightarrow(\leftarrow)} \geq +(-)\Delta G_{\rm FU}$, so the average dissipated work fulfills $\langle W_d\rangle_{\rightarrow(\leftarrow)} = \langle W\rangle_{\rightarrow(\leftarrow)} - (+)\Delta G_{\rm FU} \geq 0$, vanishing for a quasistatic process (i.e., infinitely slow pulling or $r \to 0$). If the loading rate is not too high, the molecule can unfold and refold more than once, the average dissipated work being typically small $\langle W_d\rangle \sim k_B T$. For higher loading rates, the process becomes irreversible, and the thermally activated unfolding tends to occur at higher forces while the refolding occurs at lower forces, increasing the average dissipation $\langle W_d\rangle \geq 0$. The Crooks FT and the Jarzynski equality, that is Eq. (1) with $\gamma = 1$ and Eq. (8) with $\Upsilon_M = 0$, are fulfilled because no feedback is involved.

C. Mean-field approximation

Neglecting multiple hopping transitions between F and U along $\rightarrow$ ($\leftarrow$) implies that, once the molecule jumps to U (F) at a given λ, it remains in that state until reaching $\lambda_{\rm max}$ ($\lambda_{\rm min}$). Therefore, we identify $\psi(\lambda) = c \times p^F_{\rightarrow}(\lambda, r_F) p^U_{\rightarrow}(\lambda, r_F)$ and $\tilde{\psi}(\lambda) = c' \times p^F_{\leftarrow}(\lambda, r_F) p^U_{\leftarrow}(\lambda, r_F)$, where ψ ($\tilde{\psi}$) is the normalized probability along $\rightarrow$ ($\leftarrow$) to observe U at a given value of λ for the first (last) time at the single loading (unloading) rate r_F, and $p^{\sigma}_{\rightarrow(\leftarrow)}(\lambda, r)$ is the fraction of trajectories observed in $\sigma(= F, U)$ at λ with loading rate r. c and c' are normalizing factors. Terms $J(\lambda)$, Υ_∞ in Eqs. (16b) and (17b) give

$$J_{\rm MFA}(\lambda) = I_F(\lambda) + I_U(\lambda) + \log\left(\frac{c'}{c}\right), \tag{7a}$$

$$\Upsilon_{\rm MFA} = \log\left(\int_{\lambda_{\rm min}}^{\lambda_{\rm max}} \psi(\lambda) e^{J_{\rm MFA}(\lambda)} d\lambda\right) = \log\left(\frac{\int_{\lambda_{\rm min}}^{\lambda_{\rm max}} p^F_{\leftarrow}(\lambda, r_F) p^U_{\leftarrow}(\lambda, r_U) d\lambda}{\int_{\lambda_{\rm min}}^{\lambda_{\rm max}} p^F_{\leftarrow}(\lambda, r_F) p^U_{\leftarrow}(\lambda, r_F) d\lambda}\right) \tag{7b}$$

with $I_F(\lambda)$ and $I_U(\lambda)$ in Eq. (7a) the partial thermodynamic information as in Eq. (12) for DTF at a given λ. For the experiments of hairpin $L4$, the transition state is located at half-distance of the molecular extension, resulting in nearly symmetric forward and reverse processes without feedback. Therefore, $c' \cong c$ and $\log(c'/c) \cong 0$. Equation (7a) shows $J_{\rm MFA}(\lambda)$ in CTF equals the sum of the $I_\sigma(\lambda)$ corresponding to DTF. $\Upsilon_{\rm MFA}$ in Eq. (7b) is a good approximation for Υ_∞ under highly irreversible pulling conditions where the molecule executes a single unfolding

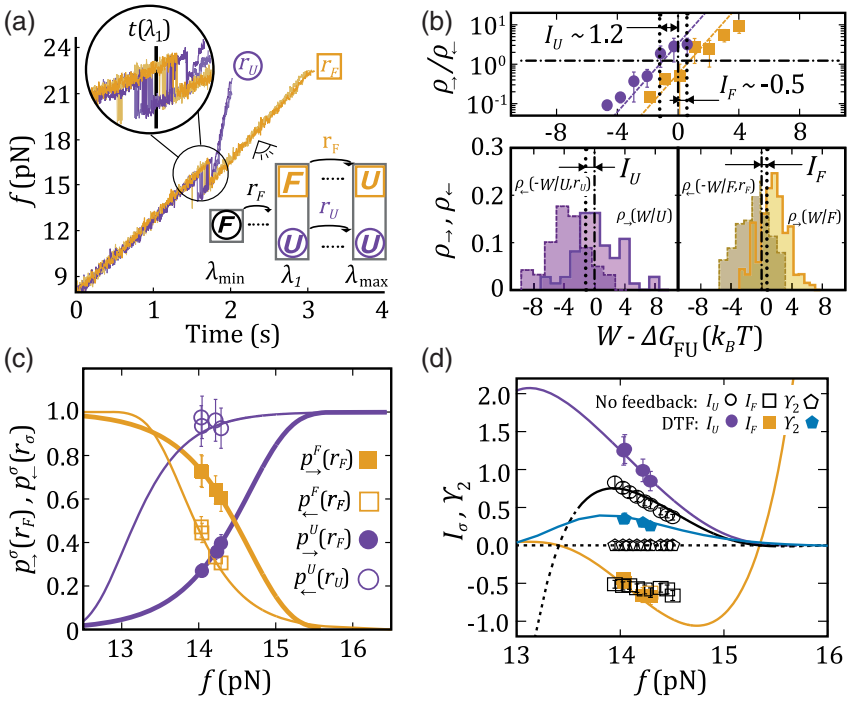

FIG. 2. Discrete-time feedback. (a) Experimental force-time unfolding curves. The molecule is pulled at $r_F = 4$ pN/s, and the observation is made at λ_1: If the molecule is folded ($\sigma = F$), the pulling rate remains unchanged ($r = r_F$, orange curves); if it is unfolded ($\sigma = U$), the pulling rate is changed to $r_U = 17$ pN/s, making refolding events less likely (purple curves). The schematic summarizes the feedback protocol and the reaction to the measurement outcome. (b) Bottom: detailed-feedback FT. $\rho_{\rightarrow}(W|\sigma)$ (solid lines) and $\rho_{\leftarrow}(-W|\sigma, r_\sigma)$ (dashed lines) for $\sigma = F, U$ (orange, purple) trajectories. Top: test of the detailed-feedback FT Eq. (12) for $\sigma = F, U$. (c) Probabilities $p^{\sigma}_{\rightarrow}(r_F)$, $p^{\sigma}_{\leftarrow}(r_\sigma)$, and (d) information terms I_σ and Υ_2 as a function of the force in U measured at λ_1. Orange (purple) data are for $\sigma = F(U)$. In (d), we also show I_σ without feedback (empty symbols). Theoretical predictions from the Bell-Evans model are shown as solid lines in (c),(d).

(folding) transition during $\rightarrow$ ($\leftarrow$). Equations (7a) and (7b) can be approximated using the Bell-Evans model for $p^{\sigma}_{\rightarrow(\leftarrow)}(\lambda, r)$ as shown in Figs. 2(c) and 4(c).

III. RESULTS

A. First-time feedback

To address DTF and CTF in full generality, we introduce the FTF protocol, a repeated-time feedback protocol suitable for pulling experiments [Fig. 1(d)] that interpolates between DTF and CTF. In the FTF protocol, the trap-position range $[\lambda_{\min}, \lambda_{\max}]$ is discretized in $M+1$ steps, $\{\lambda_k; 0 \le k \le M\}$ with boundaries $\lambda_0 = \lambda_{\min}$; $\lambda_M = \lambda_{\max}$. The feedback protocol needs at least one intermediate measure position, so $M \ge 2$. The initially folded (F) molecule is pulled at a loading rate r_F, and measurements are taken at every discrete position λ_k along the forward ($\rightarrow$) process [Fig. 1(d)]. The state $\sigma_k (= F, U)$ is monitored at every λ_k until a λ_{k^*} is reached where the molecule is observed to be in U for the first time $\{\sigma_{k^*} = U; \sigma_k = F, 0 \le k < k^*\}$. At λ_{k^*}, the loading rate is changed to r_U [Fig. 1(d), top]. Like in generic isothermal feedback processes, the conditional reverse ($\leftarrow$) process is the time reverse of $\rightarrow$ [9]: The unloading rate is equal to r_U from $\lambda_{\max}$ to λ_{k^*}, after which the unloading rate is changed back to r_F between λ_{k^*} and $\lambda_{\min}$ [Fig. 1(d), bottom]. Therefore, no feedback is implemented on $\leftarrow$. Let $p^{\sigma}_{\rightarrow,k}(r)[p^{\sigma}_{\leftarrow,k}(r)]$ be the probability to observe the molecule in state σ (F or U) at λ_k along $\rightarrow$ ($\leftarrow$) at the pulling rate r. We derive a detailed- and full-work FT for FTF (Appendix A). The full-work FT reads

$$\frac{\rho_{\rightarrow}(W)}{\rho_{\leftarrow}(-W)} = \exp\left[\frac{W - \Delta G_{\mathrm{FU}} + k_B T \Upsilon_M}{k_B T}\right]$$
$$\text{with} \quad \Upsilon_M = \log\left(\sum_{k=1}^{M} \frac{p^{U}_{\leftarrow,k}(r_U)}{p^{U}_{\leftarrow,k}(r_F)} \tilde{\psi}_k\right). \tag{8}$$

W is the work measured between $\lambda_{\min}$ and $\lambda_{\max}$ (Sec. II B), while ΔG_{FU} is the free-energy difference between the state U at $\lambda_{\max}$ and the state F at $\lambda_{\min}$, $\Delta G_{\mathrm{FU}} = G_U(\lambda_{\max}) - G_F(\lambda_{\min})$. Work distributions are given by

$$\rho_{\rightarrow}(W) = \sum_{k=1}^{M} \rho_{\rightarrow}(W|k)\psi_k, \tag{9}$$

TABLE I. Probabilities and densities in the different protocols, Probabilities (a)–(d) must be measured to calculate the corresponding densities $\rho_{\rightarrow}(W|k)$, $\rho_{\leftarrow}(-W|k)$, verify the feedback FT, and extract partial and full thermodynamic information J, Υ [columns (e),(f)]. All quantities are properly normalized in FTF: $\sum_\sigma p^\sigma_{\rightarrow,k}(r) = \sum_\sigma p^\sigma_{\leftarrow,k}(r) = \int dW \rho_{\rightarrow}(W|k) = \int dW \rho_{\leftarrow}(-W|k) = 1$ for all k and $\sum_{k=1}^M \psi_k = \sum_{k=1}^M \tilde{\psi}_k = 1$; $\int dW \rho_{\rightarrow}(W) = \int dW \rho_{\leftarrow}(-W) = 1$. Distributions in CTF are also normalized: $\int p^U_{\rightarrow,\leftarrow}(\lambda, r) d\lambda = \int \psi d\lambda = \int \tilde{\psi} d\lambda = 1$; $\int dW \rho_{\rightarrow,\leftarrow} = 1$.

Protocol	(a)	(b)	(c)	(d)	(e)	(f)
FTF	$p^\sigma_{\rightarrow,k}(r)$	$p^\sigma_{\leftarrow,k}(r)$	ψ_k	$\tilde{\psi}_k$	J_k	Υ_M
DTF	$p^\sigma_{\rightarrow}(r_F)$	$p^\sigma_{\leftarrow}(r_U)$	$\psi_1 = p^U_{\rightarrow}(r_F)$ $\psi_2 = p^F_{\rightarrow}(r_F)$	$\tilde{\psi}_1 = p^U_{\leftarrow}(r_F)$ $\tilde{\psi}_2 = p^F_{\leftarrow}(r_F)$	$J_1 = I_U$ $J_2 = I_F$	Υ_2
CTF	$p^U_{\rightarrow}(r_F)$	$p^U_{\leftarrow}(\lambda, r_U)$ $p^U_{\leftarrow}(\lambda, r_F)$	$\psi(\lambda)$	$\tilde{\psi}(\lambda)$	$J(\lambda)$	Υ_∞

$$\rho_{\leftarrow}(-W) = e^{-\Upsilon_M} \sum_{k=1}^{M} \rho_{\leftarrow}(-W|k) \frac{p^U_{\leftarrow,k}(r_U)}{p^U_{\leftarrow,k}(r_F)} \tilde{\psi}_k. \tag{10}$$

Here, $\rho_{\rightarrow}(W|k)$ and $\rho_{\leftarrow}(-W|k)$ are the partial work distributions along $\rightarrow$ and $\leftarrow$ conditioned to those $\rightarrow$ paths where U is observed for the first time at λ_k. ψ_k ($\tilde{\psi}_k$) ($1 \leq k \leq M$) is the probability along $\rightarrow$ ($\leftarrow$) to observe U at λ_k for the first (last) time at the single loading (unloading) rate r_F. Note that while ψ_k can be measured from $\rightarrow$ pulls with the feedback on, the *reverse* quantities $\tilde{\psi}_k$, $p^U_{\leftarrow,k}(r_F)$, and $p^U_{\leftarrow,k}(r_U)$ are measured from reverse pulls at either the unloading rates r_F or r_U without feedback. Table I summarizes these definitions. Υ_M in Eq. (8) denotes the thermodynamic information,

$$\Upsilon_M = \log\left(\sum_{k=1}^{M} \psi_k \exp J_k\right)$$
$$\text{with} \quad J_k = \log\left(\frac{p^U_{\leftarrow,k}(r_U)\tilde{\psi}_k}{p^U_{\leftarrow,k}(r_F)\psi_k}\right), \tag{11}$$

where J_k is the *partial* thermodynamic information along $\rightarrow$, restricted to those paths where U is observed for the first time at λ_k. Equation (11) expresses Υ_M as a partition sum or potential of mean force over the partial contributions J_k. Note that for $r_U = r_F$, $J_k = \log(\tilde{\psi}_k/\psi_k)$ and $\Upsilon_M = \log(\sum_{k=1}^M \tilde{\psi}_k) = 0$. In this case, feedback is without effect and Crooks FT [56] is recovered. The FTF protocol has DTF and CTF as particular cases: DTF corresponds to $M = 2$, whereas $M \to \infty$ yields CTF.

Let us assume that the time between consecutive measurements at λ_k is equal to τ, in which case $M \to \infty$ corresponds to $\tau \to 0$. To implement CTF experimentally, we take the lowest possible value of τ as dictated by the maximum data acquisition frequency of the instrument ($\tau \approx 1$ ms). Below we report feedback experiments in DTF and CTF and measure Υ, η_I, and η_M in the regime $r_U > r_F$.

B. Discrete-time feedback ($M = 2$)

In DTF, the pulling rate along $\rightarrow$ is changed from r_F to r_U at a given trap position λ_1 if $\sigma = U$, otherwise, it remains unchanged [Figs. 1(c) and 2(a)]. Therefore, if $\sigma = F$ at λ_1, the pulling rate is constant and equal to r_F throughout the pulling cycle, whereas if $\sigma = U$ at λ_1, the pulling rate along $\leftarrow$ starts at $r = r_U$ and switches back to r_F at λ_1. A detailed-feedback FT can be derived either from the detailed form of Eq. (8) for $M = 2$ or from the extended fluctuation relation [50] (Table I and Appendix B)

$$\frac{\rho_{\rightarrow}(W|\sigma)}{\rho_{\leftarrow}(-W|\sigma, r_\sigma)} = \exp\left[\frac{W - \Delta G_{\mathrm{FU}} + k_B T I_\sigma}{k_B T}\right]$$
$$\text{with} \quad I_\sigma \equiv \log\left(\frac{p^\sigma_{\leftarrow}(r_\sigma)}{p^\sigma_{\rightarrow}(r_F)}\right); \qquad \sigma = \{F, U\}, \tag{12}$$

where $\sigma(= F, U)$ is the measurement outcome at λ_1 along $\rightarrow$. $\rho_{\rightarrow}(W|\sigma)$ and $\rho_{\leftarrow}(W|\sigma, r_\sigma)$ are the (normalized) work distributions conditioned to those trajectories passing through σ at λ_1 along $\rightarrow$ and $\leftarrow$, respectively. The $p^\sigma_{\rightarrow}(r_F)$, $p^\sigma_{\leftarrow}(r_\sigma)$ are the probabilities to measure σ at λ_1 along $\rightarrow$ and $\leftarrow$, at the respective pulling rates. Finally, I_σ is the partial thermodynamic information of measurement outcome σ. Note that I_σ can take any sign depending on the ratio $p^\sigma_{\leftarrow}(r_\sigma)/p^\sigma_{\rightarrow}(r_F)$, which can be larger or smaller than 1. Moreover, while all trajectories in $\rightarrow$ are classified in one of the two groups $\sigma = \{F, U\}$, only those that revisit again the same σ contribute to $\rho_{\leftarrow}(-W|\sigma, r_\sigma)$. Therefore, the normalization condition along $\rightarrow$, $\sum_\sigma p^\sigma_{\rightarrow}(r_F) = 1$ is not applicable to $\leftarrow$, i.e., $\sum_\sigma p^\sigma_{\leftarrow}(r_\sigma) \neq 1$. Equation (12) for $\sigma = \{F, U\}$ permits us to extract ΔG_{FU} from DTF experiments. First, we apply the protocol without feedback ($r_U = r_F$) as a consistency check [Fig. 1(b)]. We find that Crooks FT [56] is satisfied with work distributions ($\rightarrow$, $\leftarrow$) crossing at a ΔG_{FU} consistent with bulk predictions (Sec. S1, Supplemental Material [57]). Next, we apply DTF with $r_U > r_F$ to extract partial work distributions $\rho_{\rightarrow}(W|\sigma)$ and $\rho_{\leftarrow}(-W|\sigma, r_\sigma)$ by classifying trajectories depending on the outcome σ at λ_1 and the protocol under which they are operated. Figure 2(b) (bottom) shows results for $\sigma = F$, U for $r_F = 4$ pN/s, $r_U = 17$ pN/s. For the F (U) subset, we find that the work distributions are shifted rightward (leftward) with respect to the nonfeedback case with crossing points (W^*_σ) such that $W^*_F > \Delta G_{\mathrm{FU}}$ ($W^*_U < \Delta G_{\mathrm{FU}}$). These shifts reflect the fact that hairpin unfolding is on average more (less) energy costly for the F

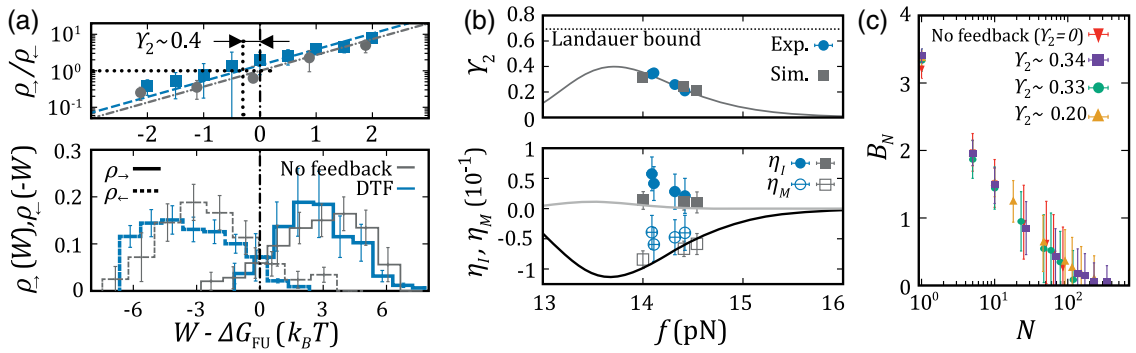

FIG. 3. DTF efficiencies η_I, η_M. (a) Top: test of the full-feedback FT Eq. (13a) with shift Υ_2 (blue) with respect to the no-feedback case (gray). Bottom: work distributions. (b) Thermodynamic information Υ_2 (top), and efficiencies η_I and η_M (bottom) are shown at different measurement positions (gray, simulations; blue, experiments). Solid lines are the Bell-Evans model in the single-hopping approximation (Appendix C). In general, Υ_2 is bounded from above by the Landauer limit for binary measurements (log 2, dashed line). (c) Bias for three different DTF conditions compared to the nonfeedback case. There is no improvement in free-energy prediction.

(U) subset than without feedback at the pulling rate r_F. From Eq. (12), the measured shift defined as $W^*_\sigma - \Delta G_{\mathrm{FU}}$ equals $-k_BTI_\sigma$. The $\rho_{\rightarrow}(W|\sigma)$ and $\rho_{\leftarrow}(-W|\sigma, r_\sigma)$ fulfill Eq. (12) crossing at values $W^*_\sigma = \Delta G_{\mathrm{FU}} - k_BTI_\sigma$ with $I_F \approx -0.5$ and $I_U \approx 1.20$ [Fig. 2(b), top]. In Figs. 2(c) and 2(d), we show $p^\sigma_{\rightarrow}(r_F)$, $p^\sigma_{\leftarrow}(r_\sigma)$, and $I_{F,U}$ versus the force in U at λ_1 together with predictions based on the Bell-Evans model (Appendix C). We choose force as a reference value to present the results. Force is more informative than the trap position λ, which is a relative distance between the trap position and an arbitrary initial position in the light-lever detector.

Combining the detailed-feedback FT Eq. (12) for $\sigma = F, U$ yields to the full-work FT Eq. (8) for $M = 2$ (Appendix B),

$$\frac{\rho_{\rightarrow}(W)}{\rho_{\leftarrow}(-W)} = \exp\left[\frac{W - \Delta G_{\mathrm{FU}} + k_BT\Upsilon_2}{k_BT}\right] \tag{13a}$$

$$\text{with} \quad \Upsilon_2 = \log\left(\sum_{\sigma=F,U} p^\sigma_{\leftarrow}(r_\sigma)\right) = \log\left(\sum_{\sigma=F,U} p^\sigma_{\rightarrow}(r_F)\exp I_\sigma\right), \tag{13b}$$

Υ_2 being the thermodynamic information. The forward and reverse work distributions are given by

$$\rho_{\rightarrow}(W) = \sum_\sigma p^\sigma_{\rightarrow}(r_F)\rho_{\rightarrow}(W|\sigma), \tag{14}$$

$$\rho_{\leftarrow}(-W) = e^{-\Upsilon_2}\sum_\sigma p^\sigma_{\leftarrow}(r_\sigma)\rho_{\leftarrow}(-W|\sigma, r_\sigma). \tag{15}$$

For $r_F = r_U$, we have $p^F_{\leftarrow}(r) + p^U_{\leftarrow}(r) = 1$ yielding $\Upsilon_2 = 0$ and Crooks FT [56] as expected. Figure 3(a) tests Eq. (13a), and Fig. 3(b) shows Υ_2 and the efficiencies η_I, η_M obtained in experiments. The results are compared with numerical simulations of the DNA pulling experiments (see details in Sec. S2 of the Supplemental Material [57]) and a prediction by the Bell-Evans model (Appendix C). For $r_U > r_F$, $p^F_{\leftarrow}(r_F) + p^U_{\leftarrow}(r_U) > 1$ and $\Upsilon_2 > 0$, whereas $\Upsilon_2 < 0$ for $r_U < r_F$. In general, $-\infty < \Upsilon_2 \le \log 2 [0 \le p^\sigma_{\leftarrow}(r_\sigma) \le 1]$ showing that the Landauer bound holds for two-state molecules pulled under DTF. Saturating the bound $\Upsilon_2 = \log 2$, requires full reversibility [44], i.e., $p^\sigma_{\leftarrow}(r_\sigma) = 1$, which is obtained for arbitrary r_F in the limit $r_U \to \infty$ $[p^U_{\leftarrow}(r_U) = 1]$ and $\lambda_1 \to \lambda_{\min}$ [i.e., maximally stable F or $p^F_{\leftarrow}(r_F) = 1$]. We find $\eta_M \approx -0.05 < \eta_I \approx 0.04$ showing that information-to-measurement conversion is much less efficient than the information-to-work conversion. Moreover, $\eta_M < 0$ throughout the whole force range shows that DTF does not improve free-energy prediction.

To better understand this result, we calculate the efficiencies η_I and η_M for DTF in the two-states Bell-Evans model using the single-hopping approximation (Appendix C). Figure 3(b) shows that the analytical results capture the trend of the experimental data but systematically underestimate the measured efficiencies η_I and η_M. As we explain in Appendix C, the single-hopping approximation neglects multiple transitions after the measurement position at λ_1. Therefore, the analytical results derived in Eqs. (C1)–(C3) in Appendix C are lower bounds to the true efficiencies. The fact that $\eta_M < 0$ throughout the force range shows that although DTF does reduce dissipation, it does not improve the free-energy prediction. This conclusion is supported by the results shown in Fig. 3(c). There we plot the experimental free-energy bias Eq. (4) as a function of the number of pulling experiments N at the conditions shown in Fig. 3(b): Bias with feedback does not decrease with respect to the nonfeedback case (downward-pointing red triangles).

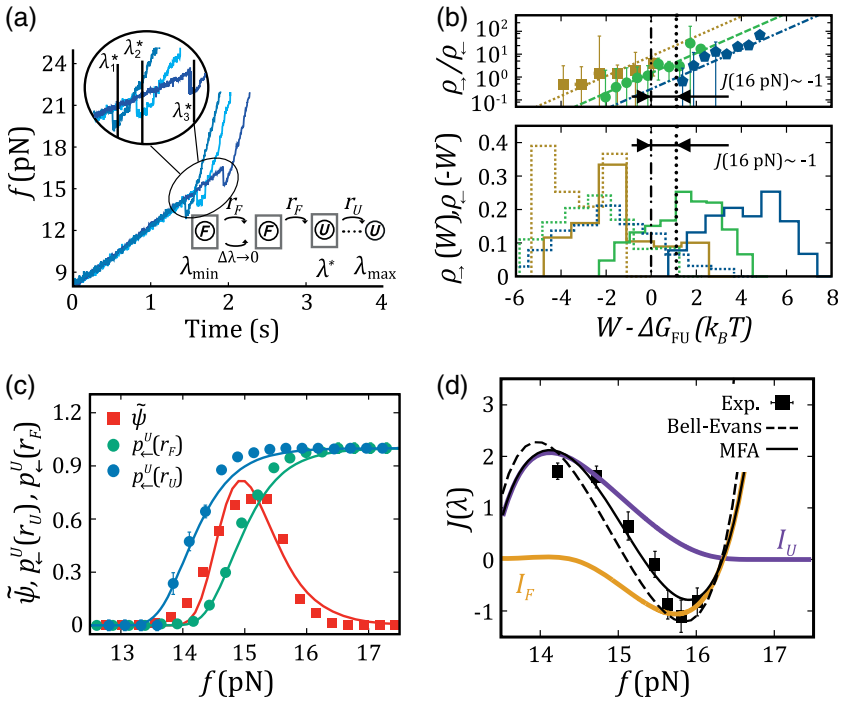

FIG. 4. Continuous-time feedback. (a) Experimental unfolding curves. The molecule is pulled at $r_F = 5$ pN/s along $\rightarrow$. Upon detection of the first unfolding event, the pulling rate is changed to $r_U = 23$ pN/s. (b) Experimental test of the detailed-feedback FT Eq. (16a) and measurement of $J(\lambda)$. FDCs are classified according to the value of λ at which the earliest unfolding event is detected. FDCs are grouped in bins of equal width $\Delta\lambda \sim 6$ nm and Eq. (16a) applied to each interval. We show work histograms for three different bins. The value of $J(\lambda)$ for the bin corresponding to $f = 16$ pN is highlighted. We use force due to its one-to-one correspondence along the folded branch with λ. (c) $p^U_{\leftarrow}(\lambda, r_U)$, $p^U_{\leftarrow}(\lambda, r_F)$, and last-folding density $\tilde{\psi}(\lambda)$. Solid lines correspond to fits to the Bell-Evans model. (d) The $J(\lambda)$ from the detailed-feedback FT Eq. (16a) (squares) obtained from the data in panel (b) compared to the theoretical prediction by the Bell-Evans model (c) applying Eq. (16b) (dashed line). Also, the MFA approximation Eq. (7a) with $\log(c'/c) \sim 0$ is shown as a solid line. $I_F(\lambda)$ (orange) and $I_U(\lambda)$ (purple) are from Eq. (12) using the Bell-Evans model. The values of $p^U_{\leftarrow}(r_U)$, $p^U_{\leftarrow}(r_F)$, $\tilde{\psi}$, J, I_F, I_U in (c),(d) are plotted versus $f(\lambda)$.

C. Continuous-time feedback ($M \to \infty$)

CTF [Figs. 1(c) and 4(a)] is obtained from Eqs. (8) and (11) in the limit of $\Delta\lambda(=\lambda_{k+1} - \lambda_k)$, $\tau \to 0$. The detailed-feedback FT reads (Table I and Appendix A)

$$\frac{\rho_{\rightarrow}(W|\lambda)}{\rho_{\leftarrow}(-W|\lambda)} = \exp\left[\frac{W - \Delta G_{\mathrm{FU}} + k_B T J(\lambda)}{k_B T}\right], \tag{16a}$$

$$J(\lambda) = \log\left(\frac{p^U_{\leftarrow}(\lambda, r_U)\tilde{\psi}(\lambda)}{p^U_{\leftarrow}(\lambda, r_F)\psi(\lambda)}\right), \tag{16b}$$

while the full-feedback FT reads

$$\frac{\rho_{\rightarrow}(W)}{\rho_{\leftarrow}(-W)} = \exp\left[\frac{W - \Delta G_{\mathrm{FU}} + k_B T \Upsilon_\infty}{k_B T}\right], \tag{17a}$$

$$\Upsilon_\infty = \log\left(\int_{\lambda_{\min}}^{\lambda_{\max}} \frac{p^U_{\leftarrow}(\lambda, r_U)}{p^U_{\leftarrow}(\lambda, r_F)}\tilde{\psi}(\lambda)d\lambda\right) = \log\left(\int_{\lambda_{\min}}^{\lambda_{\max}} \psi(\lambda)\exp J(\lambda)d\lambda\right) \tag{17b}$$

with the forward and reverse work distributions given by

$$\rho_{\rightarrow}(W) = \int_{\lambda_{\min}}^{\lambda_{\max}} \rho_{\rightarrow}(W|\lambda)\psi(\lambda)d\lambda, \tag{18}$$

$$\rho_{\leftarrow}(-W) = e^{-\Upsilon_\infty}\int_{\lambda_{\min}}^{\lambda_{\max}} \rho_{\leftarrow}(-W|\lambda) \times \frac{p^U_{\leftarrow}(\lambda, r_U)}{p^U_{\leftarrow}(\lambda, r_F)}\tilde{\psi}(\lambda)d\lambda, \tag{19}$$

where $\psi(\lambda)$ [$\tilde{\psi}(\lambda)$] is the probability density to observe the first (last) unfolding (folding) event $F \to U$ ($F \leftarrow U$) along $\rightarrow$ ($\leftarrow$); $p^U_{\leftarrow}(\lambda, r)$ is the probability density of the molecule being in U at λ along $\leftarrow$ at the unloading rate r. Similar to I_σ in Eq. (12), if we define $I^{rr'}_\sigma(\lambda) = \log[p^\sigma_{\leftarrow}(\lambda, r')/p^\sigma_{\rightarrow}(\lambda, r)]$, we have $J(\lambda) = I^{r_F r_U}_U(\lambda) - I^{r_F r_F}_U(\lambda) + I_\psi(\lambda)$ with $I_\psi(\lambda) = \log[\tilde{\psi}(\lambda)/\psi(\lambda)]$. Notice that for $r_U = r_F$ (no feedback), $\rho_{\leftarrow}(-W|\lambda) = \rho_{\leftarrow}(-W)$ and $\Upsilon_\infty = 0$, but $J(\lambda) = I_\psi(\lambda) \neq 0$. Equations (16b) and (17b) can be further simplified by neglecting multiple hopping transitions between F and U. In this mean-field approximation (MFA), $J(\lambda)$ interpolates the I_σ in Eq. (12) and Υ_∞ depends only on the $p_{\leftarrow}(\lambda, r)$ (Sec. II C).

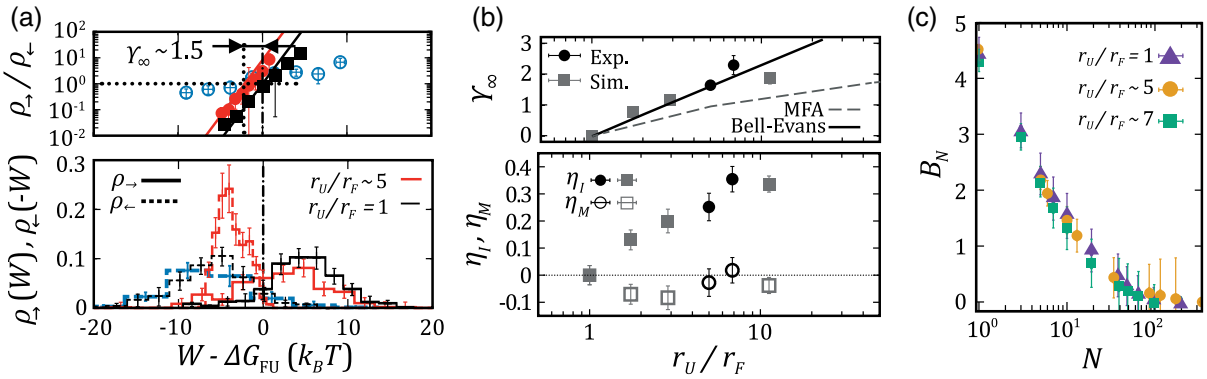

FIG. 5. CTF efficiencies η_I, η_M. (a) Top: test of the full-feedback FT Eq. (17a) (red circles) with shift Υ_∞ with respect to the nonfeedback case (black squares). Blue circles show a negative test with an unweighed reverse work distribution (see text). Bottom: work distributions. (b) Top: thermodynamic information Υ_∞ and (bottom) efficiencies η_I and η_M from the experimental data (circles) and simulations (squares) versus r_U/r_F. We also show the theoretical predictions for Υ_∞, Eq. (17b), using $p^U_\leftarrow(r_U)$, $p^U_\leftarrow(r_F)$, $\tilde{\psi}$ from Fig. 4(c) (continuous lines) and the MFA Eq. (7b) (dashed line). Notice that Υ_∞ is unbounded from above and $\eta_M < 0$. (c) Bias for the studied molecules with CTF (squares, circle) compared with the nonfeedback case. There is no improvement in free-energy prediction.

We test CTF in DNA hairpin pulling experiments [Fig. 4(a)]. The molecule initially in F is pulled from $f_{\rm min} = 8$ pN at $r_F = 5$ pN/s and the state monitored by recording the force every $\tau = 1$ ms until the first force jump is observed at a given trap position λ^*. The force rip corresponds to the unzipping of the 44 nucleotides of the DNA hairpin and indicates that state U has been visited for the first time at λ^*. Then the pulling rate is increased to $r_U = 23$ pN/s until the maximum force is reached, $f_{\rm max} = 22$ pN. For the reverse process, the optical trap moves backward at $r_U = 23$ pN/s until λ^* is reached and the pulling rate switched back to $r_F = 5$ pN/s. By repeatedly pulling, we collect enough statistics to test Eqs. (16a) and (17a) and measure $J(\lambda)$ and Υ_∞. In Fig. 4(b) (bottom), we plot $\rho_\rightarrow(W|\lambda)$, $\rho_\leftarrow(-W|\lambda)$ for three selected λ^*, while in the top panel we test Eq. (16a). By determining the crossing work values between $\rho_\rightarrow$ and $\rho_\leftarrow$, $W^*(\lambda) = \Delta G_{\rm FU} - k_BTJ(\lambda)$, we extract $J(\lambda)$.

Figure 4(c) shows the values of $\tilde{\psi}$ and $p^U_\leftarrow$ directly determined from experimental FDCs for the two loading rates, $r_F = 5$ pN/s and $r_U = 23$ pN/s (symbols) as a function of the force. The $p^U_\leftarrow$ values are fitted to the Bell-Evans model (solid lines) to extract the kinetic parameters of hairpin $L4$, useful to compare with the simulations. Figure 4(d) shows the experimental values of $J(\lambda)$ determined from the detailed-feedback FT Eq. (16a) (filled squares) together with the predictions by the fits to the Bell-Evans model using Eq. (16b) (dashed line) and the MFA Eq. (7a) assuming that $\log(c'/c) = 0$ (solid line).

In Fig. 5(a), we test the full-feedback FT Eq. (17a). For comparison, we also show the nonfeedback case. We emphasize the importance of properly weighing $\rho_\leftarrow(-W|\lambda)$ to build $\rho_\leftarrow(-W)$. An *unweighted* reverse work distribution [$\int \rho_\leftarrow(-W|\lambda)d\lambda$, blue] does not fulfill the FT (inset, blue points), and the slope of the fitting line (approximately 0.08) is far below 1. Figure 5(b) (top) shows Υ_∞ for different experimental conditions (black circles) and results obtained in simulations (gray squares) of a hairpin model (Sec. S2, Supplemental Material [57]) compared to the theoretical values determined from Eq. (17b) using the Bell-Evans model fits of Fig. 4(c). Also, the MFA using Eq. (7b) is shown as a dashed line. In Fig. 5(b) (bottom), we show the efficiencies η_I and η_M versus r_U/r_F. As shown in Fig. 5(b), dissipation reduction is larger for CTF as compared to DTF (for CTF, $\Delta\langle W_d\rangle$ is not bounded by the Landauer limit $k_BT\log 2$). However, $\eta_M \sim -0.1$ is slightly negative as in DTF, showing that dissipation reduction does not necessarily improve free-energy determination. In Fig. 5(c), we plot the experimental free-energy bias Eq. (4) as a function of the number of pulling experiments N at the conditions shown in Fig. 5(b): As for DTF, we observe that the bias with feedback does not decrease relative to the nonfeedback case (purple triangles).

D. Inefficient information-to-measurement conversion

By reducing dissipation, feedback might be used to improve free-energy prediction. Second laws inequality Eq. (2) permits us to reduce $\langle W_d\rangle$ with respect to the bound without feedback $\langle W_d\rangle_0 \geq 0$. However, this is not true if the reduction in work is lower than the thermodynamic information: $\langle W_d\rangle + k_BT\Upsilon \geq \langle W_d\rangle_0$ and $\eta_M \leq 0$. Then, the Jarzynski bias for Eq. (6) increases with feedback undermining free-energy determination [53]. This is the case of the DTF and CTF experiments previously shown.

Hairpin $L4$ exhibits low dissipation without feedback. Here we ask whether feedback efficiency increases upon increasing the irreversibility of the process ($\langle W_d\rangle_0$ larger). For this, we carry out numerical simulations of the phenomenological model for a new DNA hairpin ($L8$). $L8$ has the same stem as the previous hairpin [$L4$, Fig. 1(a)] but with an eight-bases loop. $L8$ shows larger dissipation

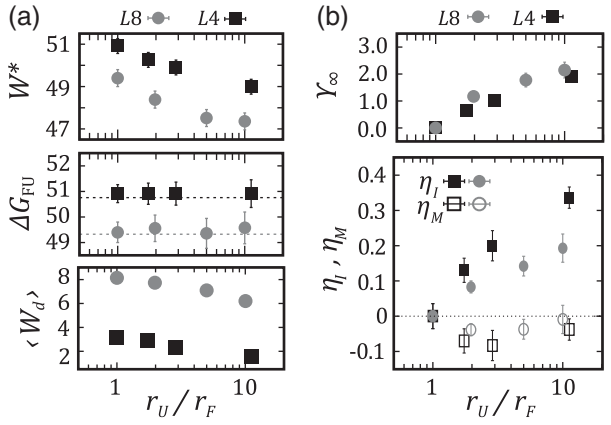

FIG. 6. Free-energy prediction with CTF. (a) Values for W^* (top), ΔG_{FU} (middle), and $\langle W_d \rangle$ (bottom) for hairpins $L4$ and $L8$. ΔG_{FU} values are obtained by adding Υ_∞ [panel (b)] and the crossing work values W^*, $\Delta G_{\mathrm{FU}} = W^* + k_B T \Upsilon_\infty$, and are compared to the correct free-energy values (dashed lines in ΔG_{FU}). (b) Values for Υ_∞ Eq. (17c), η_I and η_M Eqs. (3) and (6) versus r_U/r_F. The values of W^*, $\langle W_d \rangle = \langle W \rangle - \Delta G_{\mathrm{FU}}$, and Υ_∞ equally decrease and increase with r_U/r_F. All energy values are in $k_B T$ units.

compared to $L4$ when pulled under the same experimental CTF protocol [Fig. 4(a)]. The results for the pulling curves $\tilde{\psi}$, $p^U_{\leftarrow}$, and the test of the full-feedback FT Eq. (17a) are shown in Sec. S3 in the Supplemental Material [57] for hairpins $L4$ and $L8$. Figure 6 summarizes the main results obtained from the simulations for $L4$ and $L8$ under CTF (Sec. S3, Supplemental Material [57]) by varying r_U for a fixed r_F. We show the values of $W^* = \Delta G_{\mathrm{FU}} - k_B T \Upsilon_\infty$ [Fig. 6(a), top] derived from the crossing point of forward and reverse work distributions from the full-feedback FT; the folding free energy of the hairpin predicted by the full-feedback FT Eq. (17a) [Fig. 6(a), middle], and the average dissipated work [Fig. 6(a), bottom]. From these values, we derive the thermodynamic information Υ_∞ and the efficiencies η_I, η_M [Fig. 6(b)]. It is worth noticing that both W^* and $\langle W_d \rangle$ mildly decrease with r_U/r_F [Fig. 6(a), top and bottom]. However, the values of W^* and Υ_∞ [Fig. 6(b), top] compensate each other yielding fairly constant estimates for $\Delta G_{\mathrm{FU}} = W^* + k_B T \Upsilon_\infty$ that are compatible with the values of ΔG_{FU} used in the simulations [Fig. 6(b), middle]. Despite the larger irreversibility of $L8$, dissipation reduction defined by $\Delta \langle W_d \rangle = \langle W_d \rangle_0 - \langle W_d \rangle$ is similar for $L4$ and $L8$ [Fig. 6(a), bottom]. Moreover, also Υ_∞ [Fig. 6(b), top] remains similar for both hairpins. This shows that increased irreversibility (quantified by $\langle W_d \rangle_0$) does not necessarily imply larger $\Delta \langle W_d \rangle$ and Υ_∞. In general, despite the fact that $\langle W_d \rangle$ decreases with positive feedback, the values of W^* and Υ_∞ decrease and increase at the same rate, respectively. Therefore, $\langle W_d \rangle + k_B T \Upsilon \cong \langle W_d \rangle_0 \geq 0$: Feedback does not make the inequality imposed by the second law any weaker. Accordingly, η_M remains $\cong 0$ for all r_U/r_F values [Fig. 6(b), bottom] indicating inefficient information-to-measurement conversion. Overall, these results demonstrate that, although CTF reduces dissipation, this is compensated by an equal decrease of $W^* = \Delta G_{\mathrm{FU}} - k_B T \Upsilon_\infty$, leading to $\eta_M \cong 0$ and unimprovement in free-energy determination.

E. Efficient information-to-measurement conversion: From protocols to strategies

Here we ask under which conditions does feedback improve free-energy determination increasing η_M? As previously shown for hairpin $L8$, the irreversibility of the nonfeedback process barely changes η_M. In CTF, dissipation reduction is larger than for DTF; however, this comes at the price of a larger $k_B T \Upsilon$, leading to $\eta_M \cong 0$.

Here we explore the possibility of modifying the feedback protocols in such a way that the dissipation reduction $\Delta \langle W_d \rangle$ is maximized relative to $k_B T \Upsilon$. In nonfeedback pulling experiments, dissipation reduction can be achieved by simply decreasing the loading rate (i.e., making the process less irreversible). However, this comes at the price of an increase in the average time per pulling cycle and a decrease of the total number of pulls in a day of experiments, rendering free-energy determination inefficient. The interesting problem is to reduce dissipation with feedback, keeping the average time per pulling cycle equal or lower to the average time per pulling cycle without feedback.

In the DTF protocol, we increase the pulling rate only when the molecule is found to be in U at λ_1, while no action is taken if the molecule is in F. As shown in Appendix C [Eq. (C3)], dissipation reduction is the product of the fraction of trajectories that are in U at λ_1, $p^U_{\rightarrow}(r_F)$ and the dissipated work reduction conditioned to the U-type trajectories. At high forces, $p^U_{\rightarrow}(r_F)$ is large, whereas dissipation reduction is low [Figs. 10(c) and 11(c)]. Conversely, $p^U_{\rightarrow}(r_F)$ is small at low forces where dissipation reduction is the largest. Maximal $\Delta \langle W_d \rangle$ is found close to the coexistence force where the terms $p^U_{\rightarrow}(r_F)$ and $[\langle W_d \rangle_{U \rightarrow F \rightarrow U}(r_U) - \langle W_d \rangle_{U \rightarrow F \rightarrow U}(r_F)]$ balance. To further reduce dissipation, one might consider applying feedback also to the large set of F-type trajectories at λ_1, e.g., by reducing the pulling rate after λ_1.

To show that η_M can be positive and large, we implement a feedback strategy combining DTF and CTF. In this DTF + CTF strategy, the molecule is initially pulled at r_F with DTF until λ_1 where a observation is made. If the outcome is U, then the pulling rate is switched to $r_U > r_F$ between λ_1 and $\lambda_{\max}$. Instead, if the outcome is F, the pulling rate is reduced to $r'_F < r_F$ and the CTF protocol turned on. In this case, at the first unfolding event after λ_1, the pulling rate is switched to $r_U > r_F > r'_F$ until $\lambda_{\max}$. In the DTF + CTF protocol, both U and F trajectories contribute to reduce the dissipated work. Moreover, the values of r'_F can be chosen such that the average time per pulling trajectory is lower compared to the nonfeedback case. In Figs. 7(a) and 7(b), we show the results obtained

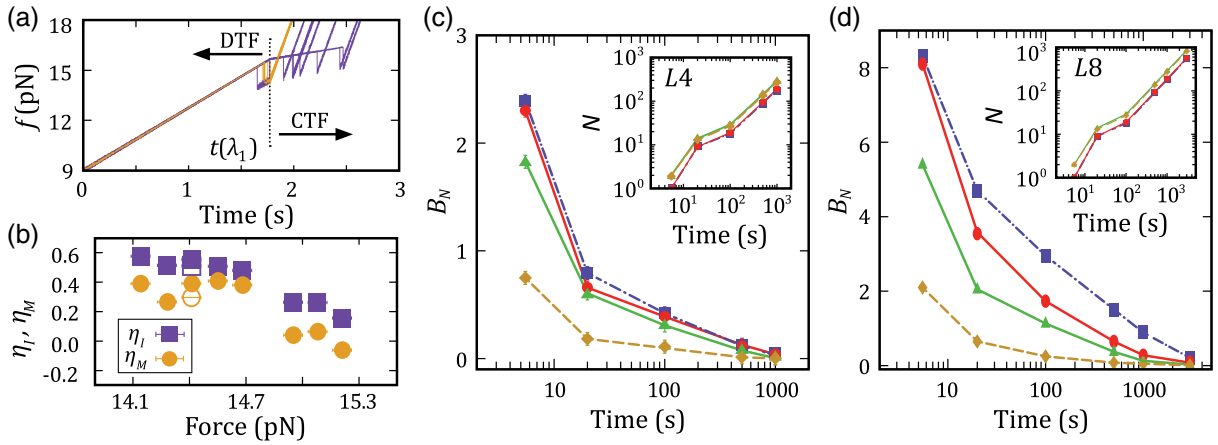

FIG. 7. DTF + CTF strategy and bias versus total experimental time. (a) Force versus time for the DTF + CTF strategy. The pulls start with DTF at $r_F = 4$ pN/s and the measurement position is at λ_1. If the molecule is observed to be in U at λ_1, the loading rate is changed to $r_U = 17$ pN/s (orange trajectories). If the molecule is observed to be in F at λ_1, the CTF is turned on with a loading rate $r'_F = 1$ pN/s $< r_F$ (purple trajectories). At the first unfolding event, the loading rate is changed from r'_F to r_U. (b) Efficiencies η_I and η_M for DTF + CTF. Solid symbols correspond to molecule $L4$, and empty symbols correspond to molecule $L8$. The values of Υ for this protocol are directly determined from the bias as we do not have an analytical expression for the thermodynamic information in this case. (c) and (d) Bias versus the experimental times measured from numerical simulations of molecule $L4$ (c) and $L8$ (d) with nonfeedback (purple), DTF (red), CTF (green), and DTF + CTF (yellow) protocols using $r_F = 4$ pN/s, $r_U = 17$ pN/s, and $r'_F = 1$ pN/s. Inset: simulated trajectories (N) for a given total experimental time. The same plots versus N (for DTF + CTF) are shown in Fig. S3 in the Supplemental Material [57].

for hairpin $L4$ in the DTF + CTF strategy where $r_F = 4 > r'_F = 1$ pN/s, $r_U = 17$ pN/s. In the coexistence force region ($f_1 \simeq 14.5$ pN) dissipated work is reduced by roughly 50%, while Υ remains unchanged with respect to the standard CTF protocol, leading to $\eta_I \sim 0.6$, $\eta_M \sim 0.4$ [Fig. 7(b)]. Similar results are obtained for $L8$ with the same rates at one specific condition. We find that B_1 decreases by approximately $1k_BT$ and approximately $6k_BT$ for $L4$ and $L8$, respectively (Sec. S4 in the Supplemental Material [57]). In addition, we compare the bias as a function of the total experimental time for the four studied protocols (nonfeedback, DTF, CTF, and DTF + CTF) from numerical simulations using molecules $L4$ and $L8$ for the same pulling rates. In Figs. 7(c) and 7(d), we show the time dependence of the bias, while in inset of Figs. 7(c) and 7(d), we present the time dependence of the number N of simulated trajectories. Although CTF generates the largest number of trajectories, the DTF + CTF strategy is the most efficient one.

F. Efficiency plot

To show all results in perspective, we introduce the efficiency plot (Fig. 8). We plot the dissipation reduction $\Delta\langle W_d\rangle = \langle W_d\rangle_0 - \langle W_d\rangle$ versus $k_BT\Upsilon$, both normalized by the nonfeedback dissipation value $\langle W_d\rangle_0$ ($\sim 2k_BT$). The results are shown for hairpin $L4$ from experiments and simulations (yellow and green symbols) for DTF and CTF (squares and circles) and DTF + CTF (red triangles), and for $L8$ at the specific DTF + CTF condition shown in Fig. 7(b). The black dashed line $\Delta\langle W_d\rangle = k_BT\Upsilon$ separates two regions: $\eta_M > 0$ (second laws weakening, yellow region) and $\eta_M < 0$ (second laws strengthening, white region). Remarkably, despite the dissipation reduction $\Delta\langle W_d\rangle > 0$, all results for DTF and CTF fall on the region $\eta_M \cong 0$ (squares and circles, dashed line), indicating that the second law is strengthened with feedback. Therefore, a large dissipation reduction (rightmost green and yellow circles) does not necessarily imply free-energy

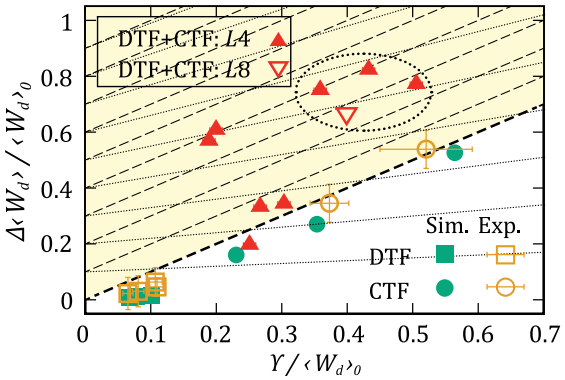

FIG. 8. Efficiency plot. Dissipation reduction $\Delta\langle W_d\rangle$ versus thermodynamic information $k_BT\Upsilon$ normalized by the nonfeedback dissipation value $\langle W_d\rangle_0$ for all explored cases in $L4$: CTF (empty circles, experimental data; full circles, simulated data), DTF (empty squares, experimental data; full square, simulated data), and the DTF + CTF strategy (red triangles). Dotted and dashed lines correspond to Eqs. (21a) and (21b) and intersect the y axis at η_I, η_M. Red empty triangles correspond to the $\Delta\langle W_d\rangle$ versus $k_BT\Upsilon$ for the $L8$ molecule under DTF + CTF protocol.

determination improvement (Sec. III D). To evaluate this, we use the definitions of η_I and η_M [Eqs. (3) and (6)] to express $\Delta\langle W_d\rangle/\langle W_d\rangle_0$ and $k_BT\Upsilon/\langle W_d\rangle_0$ as sole functions of (η_I,η_M),

$$\frac{\Delta\langle W_d\rangle}{\langle W_d\rangle_0}=\frac{\eta_I-\eta_M}{1-\eta_I}, \tag{20a}$$

$$\frac{k_BT\Upsilon}{\langle W_d\rangle_0}=\frac{\eta_I(\eta_I-\eta_M)}{1-\eta_I}, \tag{20b}$$

which for $\eta_M=0$ gives $\Delta\langle W_d\rangle=k_BT\Upsilon$ (black dashed line in Fig. 8). Efficiencies η_I, η_M separately define two linear relations between $\Delta\langle W_d\rangle/\langle W_d\rangle_0$ and $k_BT\Upsilon/\langle W_d\rangle_0$,

$$\frac{\Delta\langle W_d\rangle}{\langle W_d\rangle_0}=\eta_I+\eta_I\frac{k_BT\Upsilon}{\langle W_d\rangle_0}, \tag{21a}$$

$$\frac{\Delta\langle W_d\rangle}{\langle W_d\rangle_0}=\eta_M+\frac{k_BT\Upsilon}{\langle W_d\rangle_0}. \tag{21b}$$

These are shown as dotted [Eq. (21a)] and dashed [Eq. (21b)] lines in Fig. 8 of slopes equal to η_I and 1, and intersections with the y axis equal to η_I, η_M, respectively. For a given point in the efficiency plot, we can read the values of η_I, η_M by drawing lines of slopes η_I and 1 to match the values η_I, η_M on the y axis. As we can see, the DTF + CTF strategy yields the largest efficiencies for the largest $k_BT\Upsilon/\langle W_d\rangle_0$ values measured in CTF (circled region). The efficiency plot shows there is room for an improved free-energy prediction, opening the question of finding strategies that maximize η_M.

IV. CONCLUSIONS

We investigate dissipation reduction and information-to-measurement conversion in DNA pulling experiments with feedback. We carry out irreversible pulling experiments on DNA hairpins that are mechanically folded and unfolded, finding conditions in which feedback does reduce dissipation. In the absence of feedback, there is net dissipated work and the Jarzynski free-energy estimator is biased. We ask whether dissipation reduction can be used to improve free-energy determination by weakening the second law inequality (i.e., by a reduction of the Jarzynski bias). We find that DTF and CTF protocols mildly reduce dissipation being highly inefficient for free-energy determination. In contrast, a combination of the two protocols (denoted as a strategy) is much more efficient.

We introduce cycle efficiencies η_I, η_M for information-to-work (dissipation reduction, $\Delta\langle W_d\rangle>0$) and information-to-measurement (second law inequality weakening, $\langle W_d\rangle+k_BT\Upsilon<\langle W_d\rangle_0$) in irreversible pulling experiments with DTF and CTF. These protocols are particular cases of the FTF protocol where the pulling rate r_F switches to r_U the first time the molecule unfolds along a predetermined sequence of M measurement trap positions. A detailed- and full-feedback FT is derived for such a protocol that is expressed in terms of the free-energy difference $\Delta G_{\rm FU}$ between the unfolded and folded states [Eqs. (8) and (11)] and in terms of two new quantities, namely, the partial information J_k and the full thermodynamic information Υ_M. For $M=2$, FTF maps onto DTF [Eqs. (13a) and (13b)], the case originally considered in Refs. [11,33]. Applied to two-state molecules, DTF reduces dissipation by at most $k_BT\Upsilon_2=k_BT\log 2$ (Landauer limit). In the opposite case, $M\to\infty$, we obtain a novel-work FT for CTF Eqs. (16a) and (17a) for the partial $[J(\lambda)]$ and full thermodynamic information (Υ_∞), which is amenable to experimental test. Note that Υ_∞ is finite and unbounded, a consequence of the fact that the information content of the stored sequences diverges. The relation of Υ_M in Eq. (11) to other information-based related quantities [58–62] is an open question. Interestingly, Υ_M is reminiscent of an equilibrium free-energy potential, $G=-k_BT\log\sum_\sigma\exp\left(-G_\sigma/k_BT\right)$ with G_σ the partial free energy of state σ. By defining $g_k=J_k+\log\psi_k$, Eq. (11) can be recast as a free energy, $\Upsilon_M=\log\sum_k\exp g_k$ indicating that thermodynamic information stands for a free-energy difference.

We carry out experiments for DTF and CTF on hairpin $L4$ for pulling rates in the same range $r_F\sim 4$–5 pN/s, $r_U\sim 17$–23 pN/s. The experiments are complemented with numerical simulations of a phenomenological model for hairpins $L4$ and $L8$, and theoretical estimates of the Bell-Evans two-state model in the MFA (Sec. II C) and single-hopping (Appendix C) approximation. We find that CTF leads to higher Υ and η_I compared to DTF [Figs. 3(b) and 5(b)]. Indeed, CTF profits on early and rare unfolding events during the pulling protocol, making Υ and η_I larger, a feature also observed in a recent experimental realization of the continuous equilibrium MD [20,49]. In contrast, both DTF and CTF are inefficient regarding η_M: $\langle W_d\rangle$ decreases by roughly $k_BT\Upsilon$ leaving the second law inequality unweakened and the Jarzynski bias almost unchanged with feedback. In fact, by strategically combining DTF and CTF we can make information-to-measurement conversion efficient [Fig. 7(a)]. The DTF + CTF strategy maximizes dissipated work reduction without increasing $k_BT\Upsilon$ leading to high η_I, η_M values [Fig. 7(b)]. The results are summarized in the efficiency plot (Fig. 8), which demonstrates that efficient information-to-measurement conversion is obtained by maximizing $\Delta\langle W_d\rangle/\langle W_d\rangle_0$ while minimizing $k_BT\Upsilon/\langle W_d\rangle_0$ (ideally becoming negative). Our results show that feedback strategies (defined as a set of multiple-correlated feedback protocols) enhance the information-to-measurement efficiency, opening the door to find optimal strategies for improved free-energy determination.

Information-to-measurement conversion might be interpreted as a two-step process, with work reduction as an intermediate step of information-to-measurement conversion: Information is first used to reduce work (information-to-work conversion, $\Delta\langle W_d\rangle > 0$, efficiency η_I), followed by ΔG determination (work-to-measurement conversion, $k_B T\Upsilon$ small, efficiency η'). Therefore, $\eta_M = \eta_I\eta' \leq \eta_I, \eta' \leq 1$. These two steps must be correlated to maximize the overall efficiency, requiring multiple-correlated feedback protocols.

It would be interesting to search other nonequilibrium protocols or physical settings where $\eta_M (\lesssim \eta_I)$ is maximized. The vast majority of previous theoretical and experimental studies operate on systems that, in the absence of feedback, are in equilibrium. A handful of papers have studied dissipation reduction in nonequilibrium settings [35,63], but none of them have considered the information-to-measurement conversion. Dissipation reduction by feedback control has also been studied in macroscopic systems, e.g., feedback cooling [64], electronic and logic circuits [65], and climate change [66]. In general, feedback control corrects deviations from a reference state by monitoring the time evolution of a macroscopic observable, leading to higher dissipation. In contrast, dissipation reduction in small systems requires rectifying thermal fluctuations. It is in this context where feedback FTs are applicable.

Future studies should also address information-to-measurement conversion in systems with measurement error [67,68], non-Markovian dynamics [69,70], and biologically inspired [71–74] and mutually interacting or autonomous systems [14,16,75,76]. These examples might be tested designing single-molecule constructs containing multiple DNA structures. These studies will increase our understanding of transfer energy and information flow in nonequilibrium systems.

ACKNOWLEDGMENTS

We thank A. Alemany and J. Horowitz for their contribution in the initial stages of this work. R. K. S., J. J., and H. L. are supported by the Swedish Science Council (VR) Projects No. 2015-04105 and No. 2015-03824, and the Knut and Alice Wallenberg Foundation Project No. 2016.0089. J. M. R. P. acknowledges support from Spanish Research Council Grant No. FIS2017-83706-R. M. R.-P. and F. R. acknowledge support from European Union's Horizon 2020 Grant No. 687089, Spanish Research Council Grants No. FIS2016-80458-P and No. PID2019–111148 GB-I00, and ICREA Academia Grants 2013 and 2018.

M. R.-P. and R. K. S. contributed equally to this work.

APPENDIX A: DERIVATION OF THE FTF FT AND THE CTF LIMIT

In this section, we present the derivation of the detailed and full work FT for the FTF protocol. As a corollary, we derive the CTF limit. The derivation of the first-time FT is an application of the extended version of Crooks FT [56] introduced in Ref. [50] to reconstruct free-energy branches and applied to derive free energies of kinetic states [51] and ligand binding [52].

In pulling experiments, the force is ramped with a constant loading rate r_F. Measurements are made as a function of time or λ (natural control parameter in our optical tweezers setup). In the FTF protocol, measurements are taken at a predetermined set of trap positions along the pulling curve $\{\lambda_k; 0 \leq k \leq M\}$ at given times $\{t_k; 0 \leq k \leq M\}$ starting from an initial time $t_0 = 0$ up to a final time t_M. Therefore, there is a total number of $M-1$ observations made for each trajectory (the initial and final times are excluded) implying that $M \geq 2$.

The force and λ limits in pulling experiments are such that the molecule is always folded (F) at λ_0 and unfolded (U) at λ_M. This condition can be relaxed to include cases where the system starts either in equilibrium or in U at λ_0. However, for simplicity we stick to the scenario applicable to the experiments where the molecule always starts in F at λ_0 and always ends in U at λ_M. A measurement of the force is made at each λ_k and the state of the molecule, F or U, is determined depending on whether it falls in the folded or unfolded branch $[f_F(\lambda), f_U(\lambda)]$. Therefore, each stochastic trajectory Γ is defined by a sequence of F and U symbols, $\Gamma \equiv \{F^0, \ldots, F^{k^*-1}, U^{k^*}, \ldots, U^M\}$ $(1 \leq k^* \leq M)$. The FTF protocol changes the loading rate from the initial value r_F to a second value r_U the first time t_{k^*} an unfolding event is observed at λ_{k^*}. It is important to stress the notion of *first-time* event. In the above trajectory Γ, the first part of the sequence of measurements until position λ_k, $\{F^0, \ldots, F^{k^*-1}\}$ contains only F symbols, whereas the second part between λ_{k^*} and the limit λ_M, $\{U^{k^*}, \ldots, U^M\}$ always starts in U at λ_{k^*} and ends in U at λ_M with either none or multiple (even) hopping transitions ($F \leftrightarrow U$) in between. For example, for $M = 2$, there are two possible types of trajectories, $\{F^0, F^1, U^2\}$ and $\{F^0, U^1, U^2\}$, depending on the measurement outcome (F,U) at λ_1. $M = 2$ corresponds to the discrete-time feedback case studied in the main text. Note that the number of different measurement sequences Γ in the FTF protocol equals 2^{M-1}.

To derive the detailed-work FT, first we define the total forward work probability $\rho_{\rightarrow}(W|k^*)$ conditioned to the first unfolding event taking place at λ_{k^*} $(1 \leq k^* \leq M)$:

$$\rho_{\rightarrow}(W|k^*) = \int \prod_{k=0}^{k^*-1} [\rho_{\lambda_k \rightarrow \lambda_{k+1}}(W_{k+1}) dW_{k+1}] \times dW' \rho_{\lambda_{k^*} \rightarrow \lambda_M}(W') \delta\left(W - \sum_{k=0}^{k^*-1} W_{k+1} - W'\right). \tag{A1}$$

In Eq. (A1), $\rho_{\lambda_k \rightarrow \lambda_{k+1}}(W_{k+1})$ is the forward work distribution for the section $\lambda_k \rightarrow \lambda_{k+1}$ in the first part of the

trajectory $0 \le k \le k^* - 1$, and $\rho_{\lambda_{k^*}\to\lambda_M}(W')$ is the forward work distribution for the second part of the trajectory $\lambda_{k^*} \to \lambda_M$. Following the notation in the main text, $\lambda_0 \equiv \lambda_{\min}$ and $\lambda_M \equiv \lambda_{\max}$.

Next, we apply the detailed-work FT [50] to the work distributions measured along the two parts of trajectory Γ (before and after the first unfolding event at λ_{k^*}) and define the corresponding reverse work distributions. Notice that the reverse process is the time reverse of the forward one, meaning that the unloading rate in the reverse process equals r_U between λ_M and λ_{k^*} switching back to r_F between λ_{k^*} and λ_0. Notice there is no condition on the molecular state σ_{k^*} along the reverse process λ_{k^*}. We have

(i) Case $0 \le k \le k^* - 1$ (first part of Γ):

$$\rho_{\lambda_k\to\lambda_{k+1}}(W_{k+1}) = \rho_{\lambda_k\leftarrow\lambda_{k+1}}(-W_{k+1}) \times \exp\left[\frac{W_{k+1} - \Delta G_{\sigma_k,\sigma_{k+1}} + k_BT\log\left(\frac{\phi^{\leftarrow}_{\sigma_k}}{\phi^{\rightarrow}_{\sigma_{k+1}}}\right)}{k_BT}\right]. \tag{A2}$$

Here, $\phi^{\rightarrow}_{\sigma_{k+1}}$ is the fraction of forward trajectories that end in state σ_{k+1} at λ_{k+1} conditioned to start in state σ_k at λ_k. $\phi^{\leftarrow}_{\sigma_k}$ is the fraction of reverse trajectories that end in state σ_k at λ_k conditioned to start in state σ_{k+1} at λ_{k+1}. All these quantities (forward and reverse) are measured at pulling rate r_F. $\Delta G_{\sigma_k,\sigma_{k+1}} = G_{\sigma_{k+1}}(\lambda_{k+1}) - G_{\sigma_k}(\lambda_k)$ is the partial free-energy difference between states σ_{k+1} at λ_{k+1} and σ_k at λ_k. The partial free energy $G_\sigma(\lambda)$ of any state ($\sigma = F, U$) at a given λ equals $G_\sigma(\lambda) = -k_BT\log Z_\sigma(\lambda)$ where $Z_\sigma(\lambda)$ is the partition function restricted to the set of configurations of state σ at the trap position λ. Notice that in this first part of Γ, $\sigma_k = F$ for $0 \le k \le k^* - 1$ and $\sigma_{k^*} = U$.

(ii) Case $k^* \le k \le M$ (second part of Γ):

$$\rho_{\lambda_{k^*}\to\lambda_M}(W') = \rho_{\lambda_{k^*}\leftarrow\lambda_M}(-W') \times \exp\left[\frac{W' - \Delta G_{\sigma_{k^*},\sigma_M} + k_BT\log\left(\frac{\phi^{\leftarrow}_{\sigma_{k^*}}}{\phi^{\rightarrow}_{\sigma_M}}\right)}{k_BT}\right]. \tag{A3}$$

Here, $\phi^{\rightarrow}_{\sigma_M}$ is the fraction of forward trajectories that end in σ_M at λ_M conditioned to start in σ_{k^*} at λ_{k^*}. $\phi^{\leftarrow}_{\sigma_{k^*}}$ is the fraction of reverse trajectories that end in σ_{k^*} at λ_{k^*} conditioned to start in σ_M at λ_M. All these quantities (forward and reverse) are measured at pulling rate r_U. Note that the molecule is always in U at λ_{k^*} so $\sigma_{k^*} = U$. Moreover all pulls along the forward process end in the unfolded state at λ_M so $\sigma_M = U$ and $\phi^{\rightarrow}_{\sigma_M} = 1$ in Eq. (11). Analogously, $\Delta G_{\sigma_{k^*},\sigma_M} = \Delta G_{U,U} = G_U(\lambda_M) - G_U(\lambda_{k^*})$ is the partial free-energy difference between state U at λ_M and λ_{k^*}.

In Eqs. (A2) and (A3), k_B is the Boltzmann constant and T is the temperature. In what follows, to lighten notation we keep $\sigma_k, \sigma_{k^*}, \sigma_M$ as free variables, only at the end we replace them with $\sigma_k = F$ for $0 \le k \le k^* - 1$ and $\sigma_{k^*}, \sigma_M = U$. Inserting Eqs. (A2) and (A3) into Eq. (A1) leads to

$$\rho_{\to}(W|k^*) = \int \left[\prod_{k=0}^{k^*-1} dW_{k+1}\right] \times dW'\delta\left(W - \sum_{k=0}^{k^*-1} W_{k+1} - W'\right) AB, \tag{A4}$$

where $\beta = 1/k_BT$ and

$$B = \prod_{k=0}^{k^*-1} \rho_{\lambda_k\leftarrow\lambda_{k+1}}(-W_{k+1})\rho_{\lambda_{k^*}\leftarrow\lambda_M}(-W'), \tag{A5}$$

$$\begin{aligned} A &= \prod_{k=0}^{k^*-1} e^{\beta\left[W_{k+1} - \Delta G_{\sigma_k,\sigma_{k+1}} + k_BT\log\left(\frac{\phi^{\leftarrow}_{\sigma_k}}{\phi^{\rightarrow}_{\sigma_{k+1}}}\right)\right]} \times e^{\beta\left[W' - \Delta G_{\sigma_{k^*},\sigma_M} + k_BT\log\left(\frac{\phi^{\leftarrow}_{\sigma_{k^*}}}{\phi^{\rightarrow}_{\sigma_M}}\right)\right]} \\ &= A'A''A''' \end{aligned} \tag{A6}$$

with

$$A' = \prod_{k=0}^{k^*-1} e^{\beta W_{k+1}} e^{\beta W'} = e^{\beta\left(\sum_{k=0}^{k^*-1} W_{k+1} + W'\right)} = e^{\beta W}, \tag{A7}$$

$$\begin{aligned} A'' &= \prod_{k=0}^{k^*-1} e^{-\beta\Delta G_{\sigma_k,\sigma_{k+1}}} e^{-\beta\Delta G_{\sigma_{k^*},\sigma_M}} \\ &= e^{-\beta\sum_{k=0}^{k^*-1}\Delta G_{\sigma_k,\sigma_{k+1}} - \beta\Delta G_{\sigma_{k^*},\sigma_M}} = e^{-\beta\Delta G_{F,U}}, \end{aligned} \tag{A8}$$

$$\begin{aligned} A''' &= \prod_{k=0}^{k^*-1} e^{\beta k_BT\log\left(\frac{\phi^{\leftarrow}_{\sigma_k}}{\phi^{\rightarrow}_{\sigma_{k+1}}}\right)} e^{\beta k_BT\log\left(\frac{\phi^{\leftarrow}_{\sigma_{k^*}}}{\phi^{\rightarrow}_{\sigma_M}}\right)} \\ &= \prod_{k=0}^{k^*-1} \frac{\phi^{\leftarrow}_{\sigma_k}}{\phi^{\rightarrow}_{\sigma_{k+1}}} \times \frac{\phi^{\leftarrow}_{\sigma_{k^*}}}{\phi^{\rightarrow}_{\sigma_M}} = \frac{\prod_{k=0}^{k^*-1}\phi^{\leftarrow}_{\sigma_k}\phi^{\leftarrow}_{\sigma_{k^*}}}{\prod_{k=0}^{k^*-1}\phi^{\rightarrow}_{\sigma_{k+1}}\phi^{\rightarrow}_{\sigma_M}} \\ &= \frac{\prod_{k=0}^{k^*-2}\phi^{F,F}_{\lambda_k\leftarrow\lambda_{k+1}}}{\prod_{k=0}^{k^*-2}\phi^{F,F}_{\lambda_k\to\lambda_{k+1}}} \times \frac{\phi^{U,U,r_F}_{\lambda_{k^*}\leftarrow\lambda_M}}{\phi^{U,U,r_F}_{\lambda_{k^*}\leftarrow\lambda_M}} \times \frac{\phi^{F,U}_{\lambda_{k^*-1}\leftarrow\lambda_{k^*}}\phi^{U,U}_{\lambda_{k^*}\leftarrow\lambda_M}}{\phi^{F,U}_{\lambda_{k^*-1}\to\lambda_{k^*}}\phi^{U,U}_{\lambda_{k^*}\to\lambda_M}} \\ &= \frac{\tilde{\psi}_{k^*}}{\psi_{k^*}} \times \frac{p^U_{\leftarrow,k^*}(r_U)}{p^U_{\leftarrow,k^*}(r_F)}, \end{aligned} \tag{A9}$$

where in Eqs. (A8) and (A9), we use $\sigma_0 = F$, $\sigma_M = U$, and where we introduce in the last line of Eq. (A9) a multiplicative factor equal to 1 ($\phi^{U,U,r_F}_{\lambda_{k^*}\leftarrow\lambda_M}/\phi^{U,U,r_F}_{\lambda_{k^*}\leftarrow\lambda_M}$). Moreover, in

TABLE II. Notations.

Element	Notation in Eq. (A9)	Notation in Eqs. (A2) and (A3)	Quantity measured at
1	$\phi^{F,F}_{\lambda_k\leftarrow\lambda_{k+1}}$	$\phi^{\leftarrow}_{\sigma_k}$ with $\sigma_k=\sigma_{k+1}=F$	r_F
2	$\phi^{F,F}_{\lambda_k\rightarrow\lambda_{k+1}}$	$\phi^{\rightarrow}_{\sigma_{k+1}}$ with $\sigma_k=\sigma_{k+1}=F$	r_F
3	$\phi^{U,U,r_F}_{\lambda_{k*}\leftarrow\lambda_M}$	$\phi^{\leftarrow}_{\sigma_{k^*}}$ with $\sigma_k*=\sigma_M=U$	r_F
4	$\phi^{F,U}_{\lambda_{k^*-1}\leftarrow\lambda_{k*}}$	$\phi^{\leftarrow}_{\sigma_{k^*-1}}$ with $\sigma_{k^*-1}=F;\sigma_{k^*}=U$	r_F
5	$\phi^{F,U}_{\lambda_{k^*-1}\rightarrow\lambda_{k*}}$	$\phi^{\rightarrow}_{\sigma_{k^*}}$ with $\sigma_{k^*-1}=F;\sigma_{k^*}=U$	r_F
6	$\phi^{U,U}_{\lambda_{k^*}\leftarrow\lambda_M}$	$\phi^{\leftarrow}_{\sigma_{k*}}$ with $\sigma_k*=\sigma_M=U$	r_U
7	$\phi^{U,U}_{\lambda_{k*}\rightarrow\lambda_M}(=1)$	$\phi^{\rightarrow}_{\sigma_M}$ with $\sigma^*_k=\sigma_M=U$	r_U

the last line of Eq. (A9), we adopt a specific notation for the conditional probabilities or fractions $\phi^{\leftarrow}_{\sigma_k}$, $\phi^{\rightarrow}_{\sigma_{k+1}}$, $\phi^{\leftarrow}_{\sigma_{k^*}}$, and $\phi^{\rightarrow}_{\sigma_M}$ previously introduced in Eqs. (A2) and (A3), Table II. The conditional probabilities are as follows:

(i) $\phi^{F,F}_{\lambda_k\leftarrow\lambda_{k+1}}$ is the fraction of reverse trajectories where $\sigma_k=F$ at λ_k conditioned to $\sigma_{k+1}=F$ at λ_{k+1}. This fraction is measured with the unloading rate r_F.

(ii) $\phi^{F,F}_{\lambda_k\rightarrow\lambda_{k+1}}$ is the fraction of forward trajectories where $\sigma_{k+1}=F$ at λ_{k+1} conditioned to $\sigma_k=F$ at λ_k. This fraction is measured with the loading rate r_F.

(iii) $\phi^{U,U,r_F}_{\lambda_{k^*}\leftarrow\lambda_M}$ is the fraction of reverse trajectories where $\sigma_{k^*}=U$ at λ_{k^*} starting at $\sigma_M\equiv U$ at λ_M. As explicitly indicated in the notation, this fraction is measured at the unloading rate r_F.

(iv) $\phi^{F,U}_{\lambda_{k^*-1}\leftarrow\lambda_{k^*}}$ is the fraction of reverse trajectories where $\sigma_{k^*-1}=F$ at λ_k conditioned to $\sigma_{k^*}=U$ at λ_{k^*}. This fraction is measured with the unloading rate r_F.

(v) $\phi^{F,U}_{\lambda_{k^*-1}\rightarrow\lambda_{k^*}}$ is the fraction of forward trajectories where $\sigma_{k^*}=U$ at λ_{k^*} conditioned to $\sigma_{k^*-1}=F$ at λ_{k^*-1}. This fraction is measured with the unloading rate r_F.

(vi) $\phi^{U,U}_{\lambda_{k^*}\leftarrow\lambda_M}$ is the fraction of reverse trajectories where $\sigma_{k^*}=U$ at λ_{k^*} starting at $\sigma_M\equiv U$ at λ_M. This fraction is measured with the unloading rate r_U.

(vii) $\phi^{U,U}_{\lambda_{k^*}\rightarrow\lambda_M}$ is the fraction of forward trajectories where $\sigma_M=U$ at λ_M conditioned to $\sigma_{k^*}=U$ at λ_{k^*}. This fraction is measured with the loading rate r_U. Note that because all trajectories end in U at λ_M, the fraction $\phi^{U,U}_{\lambda_{k^*}\rightarrow\lambda_M}$ equals 1.

Note that in items 4 and 5 we introduce the quantities $\phi^{F,U}_{\lambda_{k^*-1}\leftarrow\lambda_{k^*}}$ and $\phi^{F,U}_{\lambda_{k^*-1}\rightarrow\lambda_{k^*}}$, both measured with the loading rate r_F.

To demonstrate the last equality in the last line of Eq. (A9), we group into a single product all fractions of reverse transitions at the unloading rate r_F in the numerator ($\phi^{F,F}_{\lambda_k\leftarrow\lambda_{k+1}}$, $\phi^{F,U}_{\lambda_{k^*-1}\leftarrow\lambda_{k^*}}$, $\phi^{U,U,r_F}_{\lambda_{k^*}\leftarrow\lambda_M}$), and all fractions of forward transitions at the unloading rate r_F in the denominator ($\phi^{F,F}_{\lambda_k\rightarrow\lambda_{k+1}}$, $\phi^{F,U}_{\lambda_{k^*-1}\rightarrow\lambda_{k^*}}$). We define

$$\prod_{k=0}^{k^*-2}\phi^{F,F}_{\lambda_k\rightarrow\lambda_{k+1}}\times\phi^{F,U}_{\lambda_{k^*-1}\rightarrow\lambda_{k^*}}\phi^{U,U}_{\lambda_{k^*}\rightarrow\lambda_M}=\psi_{k^*},$$
$$\prod_{k=0}^{k^*-2}\phi^{F,F}_{\lambda_k\leftarrow\lambda_{k+1}}\times\phi^{F,U}_{\lambda_{k^*-1}\leftarrow\lambda_{k^*}}\phi^{U,U,r_F}_{\lambda_{k^*}\leftarrow\lambda_M}=\tilde{\psi}_{k^*}. \tag{A10}$$

$\psi_{k^*}(1\le k^*\le M)$ is the fraction of forward trajectories that start in F at λ_0 and are observed to be in U for the first time at λ_{k^*} with loading rate r_F. $\tilde{\psi}_{k^*}(1\le k^*\le M)$ is the fraction of reverse trajectories that start in U at λ_M and are observed to be in U for the last time at λ_{k^*} with unloading rate r_F. Note that in Eq. (A10) we introduce the innocuous term for ψ_{k^*}, $\phi^{U,U}_{\lambda_{k^*}\rightarrow\lambda_M}=1$ in such a way that ψ_{k^*} is the probability of full sequences Γ (from $k=0$ to M) fulfilling the first-time condition. For $k^*=1$, the products $\prod_{k=0}^{k^*-2}$ in Eq. (A10) are equal to 1. We stress two facts: (i) both $\psi_{k^*},\tilde{\psi}_{k^*}$ are fractions measured at the single pulling rate r_F without feedback, and (ii) the notion of first and last time is bound to trajectories Γ defined as sequences of observations at the predetermination measurement positions λ_k as they are defined in the FTF protocol, irrespective of what is the state of the molecule at other intermediate (unobserved) positions.

Finally, in Eq. (A9), $\phi^{U,U}_{\lambda_{k^*}\leftarrow\lambda_M}=p^U_{\leftarrow,k^*}(r_U)$ is the fraction of reverse trajectories that start in U at λ_M and are observed to be in U at λ_{k^*} at the unloading rate r_U. According to this definition, we also have $\phi^{U,U,r_F}_{\lambda_{k^*}\leftarrow\lambda_M}=p^U_{\leftarrow,k^*}(r_F)$, a term which also appears in the denominator of the last fraction in Eq. (A9).

Inserting Eqs. (A7)–(A9) in Eq. (A6) and then in Eq. (A4), we notice that A can be taken out of the integral Eq. (A4). The remaining integral in Eq. (A4) contains only the term B from Eq. (A5), which yields the reverse work distribution $\rho_{\leftarrow}(-W|k^*)$. We stress that the reverse work distribution is conditioned to forward process through the first unfolding event observed at λ_{k^*} along that process. Putting everything together, we get the detailed-work FT for the FTF protocol,

$$\boxed{\frac{\rho_{\rightarrow}(W|k^*)}{\rho_{\leftarrow}(-W|k^*)} = \exp\left[\beta(W - \Delta G_{F,U} + k_B T J_{k^*})\right],}$$

$$\boxed{J_{k^*} = \log\left(\frac{\tilde{\psi}_{k^*}}{\psi_{k^*}} \times \frac{p^U_{\leftarrow,k^*}(r_U)}{p^U_{\leftarrow,k^*}(r_F)}\right)(1 \le k^* \le M).} \tag{A11}$$

Equation (A11) is the main theoretical result in this paper. J_{k^*} is denoted as partial thermodynamic information and depends on four basic quantities $[\psi_{k^*}, \tilde{\psi}_{k^*}, p^U_{\leftarrow,k^*}(r_F), p^U_{\leftarrow,k^*}(r_U)]$. These quantities can be measured in protocols without feedback at the pulling rate r_F along the forward process (ψ_{k^*}) and the reverse process $[\tilde{\psi}_{k^*}, p^U_{\leftarrow,k^*}(r_F)]$, and at the pulling rate r_U along the reverse process $[p^U_{\leftarrow,k^*}(r_U)]$.

From Eq. (A11), we derive the full-work FT for the FTF protocol. The full-work distribution in the forward process is given by

$$\begin{aligned}
\rho_{\rightarrow}(W) &= \sum_{k=1}^{M} \rho_{\rightarrow}(W|k)\psi_k \\
&= \sum_{k=1}^{M} \rho_{\leftarrow}(-W|k) e^{\beta(W - \Delta G_{\mathrm{FU}} + k_B T J_k)} \psi_k \\
&= e^{\beta(W - \Delta G_{\mathrm{FU}})} \sum_{k=1}^{M} \rho_{\leftarrow}(-W|k) e^{J_k} \psi_k \\
&= e^{\beta(W - \Delta G_{\mathrm{FU}})} \frac{\sum_{k=1}^{M} \rho_{\leftarrow}(-W|k) e^{J_k} \psi_k}{\sum_{k=1}^{M} e^{J_k} \psi_k} \sum_{k=1}^{M} e^{J_k} \psi_k,
\end{aligned} \tag{A12}$$

where in the last line we multiply and divide by the term $\sum_{k=1}^{M} e^{J_k}\psi_k$. This fact allows us to define the reverse full-work distribution for the FTF protocol,

$$\rho_{\leftarrow}(-W) = \frac{\sum_{k=1}^{M} \rho_{\leftarrow}(-W|k) e^{J_k + \log \psi_k}}{\sum_{k=1}^{M} e^{J_k + \log \psi_k}}. \tag{A13}$$

Notice that $\rho_{\leftarrow}(W)$ is properly normalized. Finally, we get

$$\boxed{\frac{\rho_{\rightarrow}(W)}{\rho_{\leftarrow}(-W)} = e^{\beta(W - \Delta G_{\mathrm{FU}} + k_B T \Upsilon_M)},} \tag{A14}$$

which is Eq. (8) in the main text. The term Υ_M is the thermodynamic information and equals

$$\Upsilon_M = \log\left[\sum_{k=1}^{M} \psi_k e^{J_k}\right] = \log\left[\sum_{k=1}^{M} \psi_k \frac{p^U_{\leftarrow,k}(r_U)}{p^U_{\leftarrow,k}(r_F)} \times \frac{\tilde{\psi}_k}{\psi_k}\right],$$

$$\boxed{\Upsilon_M = \log\left(\sum_{k=1}^{M} \frac{p^U_{\leftarrow,k}(r_U)}{p^U_{\leftarrow,k}(r_F)} \tilde{\psi}_k\right),} \tag{A15}$$

which gives Eq. (11) in the main text.

To conclude this section, we consider the CTF case corresponding to the limit $M \to \infty$ and determine the partial and full thermodynamic information $J(\lambda)$ and Υ_∞ in such a case.

In this limit, Eqs. (A1)–(A15) hold but with the continuous variable λ replacing the discrete variable k. The partial thermodynamic information J_k becomes the continuous function $J(\lambda)$ defined as

$$\boxed{J(\lambda) = \log\left(\frac{p^U_{\leftarrow}(\lambda, r_U)}{p^U_{\leftarrow}(\lambda, r_F)} \frac{\tilde{\psi}(\lambda)}{\psi(\lambda)}\right)} \tag{A16}$$

with equivalent definitions for the continuous fractions $[\psi(\lambda), \tilde{\psi}(\lambda), p^U_{\leftarrow}(\lambda, r_U), p^U_{\leftarrow}(\lambda, r_F)]$. The full thermodynamic information Υ_∞ is determined by taking the continuous limit $\lambda_{k+1} = \lambda_k + \Delta\lambda$, where $\Delta\lambda \to 0$, and writing the sum in Eq. (A15) as an integral:

$$\boxed{\Upsilon_\infty = \log\left(\int_{\lambda_{\min}}^{\lambda_{\max}} \frac{p^U_{\leftarrow}(\lambda, r_U)}{p^U_{\leftarrow}(\lambda, r_F)} \tilde{\psi}(\lambda) d\lambda\right).} \tag{A17}$$

Equations (A11), (A14), (A16), and (A17) for the continuous-time limit of CTF yield Eqs. (17a) and (17b) in the main text.

APPENDIX B: FT FOR DISCRETE-TIME FEEDBACK ($M = 2$)

In this section, we derive the FT for DTF, i.e., Eqs. (12) and (13a) in the main text. The derivation is done with two methods, either as the FTF FT for $M = 2$ or by directly applying the extended FT [50] by classifying trajectories according to the measurement outcome at the intermediate position λ_1.

We start by considering the FTF FT for $M = 2$. In this case, state measurement sequences are of the type $\Gamma = \{\sigma_0 = F, \sigma_1, \sigma_2 = U\}$ corresponding to the three different measurements trap positions (λ_k): λ_0, λ_1, and λ_2. The relevant quantities in Eqs. (A11), (A14), and (A15) are ψ_k, $\tilde{\psi}_k$, $p^U_{\leftarrow,k}(r_F)$, $p^U_{\leftarrow,k}(r_U)$ for $k = 1, 2$.

(i) Case $k = 1$ (λ_1): In this case, $p^U_{\leftarrow,1}(r_F) \neq 0$ and $p^U_{\leftarrow,1}(r_U) \neq 0$. Moreover, the fact that the molecule always starts in F (U) and ends in U (F) during the forward (reverse) process implies that the probability to observe the first (last) unfolding (refolding) event at λ_1 equals the probability that the molecule is in U at λ_1 during the forward (reverse) process. This argument holds for all pulling rate values $\psi_1 = p^U_{\rightarrow,1}(r_F)$, $\tilde{\psi}_1 = p^U_{\leftarrow,1}(r_F)$.

(ii) Case $k = 2$ ($\lambda_2 \equiv \lambda_{\max}$). By definition the probability to be in U at λ_2 equals 1 because all forward (reverse) trajectories end (start) in U, i.e., $p^U_{\leftarrow,2}(r_F) = p^U_{\leftarrow,2}(r_U) = 1$. Moreover, the fact that the molecule always starts in F (U) and ends in U

TABLE III. Fractions for DTF.

λ_1	λ_2
$p^U_{\leftarrow,1}(r_F) \neq 0$	$p^U_{\leftarrow,2}(r_F) = 1$
$p^U_{\leftarrow,1}(r_U) \neq 0$	$p^U_{\leftarrow,2}(r_U) = 1$
$\psi_1 = p^U_{\rightarrow,1}(r_F)$	$\psi_2 = p^F_{\rightarrow,1}(r_F)$
$\tilde{\psi}_1 = p^U_{\leftarrow,1}(r_F)$	$\tilde{\psi}_2 = p^F_{\leftarrow,1}(r_F)$

(F) during the forward (reverse) process implies that the probability to observe the first (last) unfolding (refolding) event at λ_2 equals the probability that the molecule is in F at λ_1 during the forward (reverse) process. This argument holds for all pulling rate values $\psi_2 = p^F_{\rightarrow,1}(r_F)$, $\tilde{\psi}_2 = p^F_{\leftarrow,1}(r_F)$.

The different values of $p^U_{\leftarrow,k}$, ψ_k, $\tilde{\psi}_k$ $(k = 1, 2)$ are presented in Table III.

From the results presented in Table III, we calculate the partial and full thermodynamic information $J_1 \equiv I_U, J_2 \equiv I_F$ [Eq. (A11)] and Υ_2 [Eq. (A15)]:

$$\boxed{I_U = J_1 = \log\left(\frac{p^U_{\leftarrow,1}(r_U)}{p^U_{\rightarrow,1}(r_F)}\right),}$$

$$\boxed{I_F = J_2 = \log\left(\frac{p^F_{\leftarrow,1}(r_F)}{p^F_{\rightarrow,1}(r_F)}\right).}$$

$$\boxed{\Upsilon_2 = \log\left[p^U_{\leftarrow,1}(r_U) + p^F_{\leftarrow,1}(r_F)\right].} \tag{B1}$$

Notice that $\rho_{\rightarrow}(W|k^*)$ in Eq. (A11) with $k^* = 1, 2$ corresponds to $\rho_{\rightarrow}(W|\sigma)$ in Eq. (12) in the main text with $\sigma = U, F$, respectively. Therefore, Eq. (A11) for $k = 1, 2$ gives Eq. (12) in the main text for $\sigma = U, F$, respectively. This completes the proof that the FTF FT for $M = 2$ equals DTF, Eqs. (12) and (13a) in the main text.

1. Alternative derivation of DTF

Alternatively, we can derive the detailed- and full-work FT in DTF by classifying the trajectories in two classes depending on the observation made at λ_1: (i) the system is in F at λ_1 or (ii) the system is in U at λ_1. We use the extended FT [50] to calculate the detailed-work FT for each class of trajectories, first between $\lambda_0 = \lambda_{\min}$ and λ_1, next between λ_1 and $\lambda_2 = \lambda_{\max}$. These results are then combined to extract the detailed-work FT for each class of trajectories for the full pulling cycle between $\lambda_0 = \lambda_{\min}$ and $\lambda_2 = \lambda_{\max}$.

The detailed-work FT in the range $\lambda_0 \rightarrow \lambda_1$ is given by [50]

$$\frac{p^F_{\rightarrow}(\lambda_1)}{p^F_{\leftarrow}(\lambda_1)}\frac{\rho_{\lambda_0,\lambda_1}(W|F)}{\rho_{\lambda_0,\lambda_1}(-W|F)} = \exp\left[\beta(W - \Delta G^{\lambda_0,\lambda_1}_{F,F})\right], \tag{B2a}$$

$$\frac{p^U_{\rightarrow}(\lambda_1)}{p^U_{\leftarrow}(\lambda_1)}\frac{\rho_{\lambda_0,\lambda_1}(W|U)}{\rho_{\lambda_0,\lambda_1}(-W|U)} = \exp\left[\beta(W - \Delta G^{\lambda_0,\lambda_1}_{F,U})\right], \tag{B2b}$$

where $\Delta G^{\lambda_0,\lambda_1}_{F,F(U)}$ is the free-energy difference between state $F(U)$ at λ_1 and state F at λ_0. $\rho_{\lambda_0,\lambda_1}(W|F(U))$ is the work distribution for the class of forward trajectories that start in F at λ_0 and end in $F(U)$ at λ_1. $\rho_{\lambda_0,\lambda_1}(-W|F(U))$ is the corresponding reverse work distribution. $p^{F(U)}_{\rightarrow}(\lambda_1)$ are the probabilities in the forward process to be in $F(U)$ at λ_1 conditioned to start in F at λ_0. $p^{F(U)}_{\leftarrow}(\lambda_1)$ are the probabilities in the reverse process to be in F at λ_0 conditioned to start in $F(U)$ at λ_1. By definition, $p^{F(U)}_{\leftarrow}(\lambda_1) = 1$ because the system always ends in F at λ_0. All quantities in Eqs. (B2a) and (B2b) are measured at the pulling rate r_F.

Analogously, the detailed-work FT in the range $\lambda_1 \rightarrow \lambda_2$ is given by [50]

$$\frac{p^F_{\rightarrow}(\lambda_1)}{p^F_{\leftarrow}(\lambda_1|r_F)}\frac{\rho_{\lambda_1,\lambda_2}(W|F)}{\rho_{\lambda_1,\lambda_2}(-W|F,r_F)} = \exp\left[\beta(W - \Delta G^{\lambda_1,\lambda_2}_{F,U})\right], \tag{B3a}$$

$$\frac{p^U_{\rightarrow}(\lambda_1)}{p^U_{\leftarrow}(\lambda_1,r_U)}\frac{\rho_{\lambda_1,\lambda_2}(W|U)}{\rho_{\lambda_1,\lambda_2}(-W|U,r_U)} = \exp\left[\beta(W - \Delta G^{\lambda_1,\lambda_2}_{U,U})\right], \tag{B3b}$$

where $\Delta G^{\lambda_1,\lambda_2}_{F(U),U}$ is the free-energy difference between state U at λ_2 and state $F(U)$ at λ_1, $\rho_{\lambda_1,\lambda_2}(W|F(U))$ is the work distribution for the class of forward trajectories that start in $F(U)$ at λ_1 and end in U at λ_2. $\rho_{\lambda_1,\lambda_2}(-W|F(U),r_{F(U)})$ is the corresponding reverse work distribution at the corresponding unloading rate r_F [Eq. (B3a)] and r_U [Eq. (B3b)]. $p^{F(U)}_{\rightarrow}(\lambda_1)$ are the probabilities in the forward process to be in U at λ_2 conditioned to start at $F(U)$ in λ_1. By definition, $p^{F(U)}_{\rightarrow}(\lambda_1) = 1$ because the system always ends in U at λ_2. $p^{F(U)}_{\leftarrow}(\lambda_1|r_{F(U)})$ are the probabilities in the reverse process to be in $F(U)$ at λ_1 conditioned to start in U at λ_2 with unloading rate r_F (r_U). The unloading rate value for quantities in the reverse process are explicitly indicated in Eqs. (B2a) and (B2b).

From Eqs. (B2a), (B2b), (B3a), and (B3b), we calculate the partial forward work distributions across the whole range $\lambda_{\min} \rightarrow \lambda_{\max}$ for the two classes of trajectories:

$$\rho_{\rightarrow}(W|F) = \int \rho_{\lambda_0,\lambda_1}(W_1|F)\rho_{\lambda_1,\lambda_2}(W_2|F) \times \delta(W - W_1 - W_2)dW_1dW_2, \tag{B4a}$$

$$\rho_{\rightarrow}(W|U) = \int \rho_{\lambda_0,\lambda_1}(W_1|U)\rho_{\lambda_1,\lambda_2}(W_2|U) \times \delta(W - W_1 - W_2)dW_1dW_2. \tag{B4b}$$

Putting everything together, we obtain the detailed-work FTs for DTF,

$$\boxed{\frac{\rho_{\rightarrow}(W|F)}{\rho_{\leftarrow}(-W|F,r_F)} = \exp\left[\beta(W-\Delta G_{\mathrm{FU}}+k_BTI_F)\right]}$$

$$\text{with} \quad \boxed{I_F = \log\left(\frac{p^F_{\leftarrow}(r_F)}{p^F_{\rightarrow}}\right),} \tag{B5a}$$

$$\boxed{\frac{\rho_{\rightarrow}(W|U)}{\rho_{\leftarrow}(-W|U,r_U)} = \exp\left[\beta(W-\Delta G_{\mathrm{FU}}+k_BTI_U)\right]}$$

$$\text{with} \quad \boxed{I_U = \log\left(\frac{p^U_{\leftarrow}(r_U)}{p^U_{\rightarrow}}\right),} \tag{B5b}$$

where $\Delta G_{\mathrm{FU}} = \Delta G^{\lambda_0,\lambda_1}_{F,U(F)} + \Delta G^{\lambda_1,\lambda_2}_{U(F),U} = G_U(\lambda_{\max}) - G_F(\lambda_{\min})$ is the full free-energy difference and where the argument λ_1 has dropped from the fractions $p^{F(U)}_{\rightarrow(\leftarrow)}(\lambda_1)$. Equations (B5a) and (B5b) are the detailed-feedback FTs reported in Eq. (12) of the main text.

From Eqs. (B5a) and (B5b), we compute the full-work FT as follows:

$$\begin{aligned}\rho_{\rightarrow}(W) &= \rho_{\rightarrow}(W|F)p^F_{\rightarrow} + \rho_{\rightarrow}(W|U)p^U_{\rightarrow} \\ &= \rho_{\leftarrow}(-W)e^{\{\beta(W-\Delta G_{\mathrm{FU}}+k_BT\log[p^F_{\leftarrow}(r_F)+p^U_{\leftarrow}(r_U)])\}},\end{aligned}$$

where

$$\rho_{\leftarrow}(-W) = \frac{[p^F_{\leftarrow}(r_F)\rho_{\leftarrow}(-W|F,r_F) + p^U_{\leftarrow}(r_U)\rho_{\leftarrow}(-W|U,r_U)]}{[p^F_{\leftarrow}(r_F)+p^U_{\leftarrow}(r_U)]}. \tag{B6}$$

Therefore, we obtain the full-work FT for DTF Eqs. (13a) and (13b) in the main text:

$$\boxed{\frac{\rho_{\rightarrow}(W)}{\rho_{\leftarrow}(-W)} = \exp\left[\beta(W-\Delta G_{\mathrm{FU}}+k_BT\Upsilon_2)\right]}$$

$$\text{with} \quad \boxed{\Upsilon_2 = \log\left[p^F_{\leftarrow}(r_F)+p^U_{\leftarrow}(r_U)\right].} \tag{B7}$$

APPENDIX C: THE BELL-EVANS MODEL IN SINGLE-HOPPING APPROXIMATION

To better understand under which conditions η_I and η_M are optimal, we carry out an analysis of DTF in the two-states Bell-Evans model where force is the control parameter. To analyze dissipation reduction, we define $\Delta\langle W_d\rangle = \langle W_d\rangle_0 - \langle W_d\rangle > 0$, the change in the average dissipated work upon implementing feedback. The Bell-Evans approximation where the force is controlled has been shown to be qualitatively identical and quantitatively comparable to the experimental condition where the trap position is controlled [77]. In Fig. 9, we show a typical trajectory (state versus force) in the DTF protocol in the model where the initially folded (F) molecule is pulled at $\dot{f} = r_F$ and the pulling rate changes to $\dot{f} = r_U$ at a given force value (f_1) if the molecule is observed to be unfolded (U). $\Delta\langle W_d\rangle$ is determined only by the contribution of those trajectories that are in U at f_1: Trajectories that are at F at f_1 do not change the pulling rate and therefore do not contribute to $\Delta\langle W_d\rangle$. To determine $\Delta\langle W_d\rangle$, we restrict the analysis to single-hopping trajectories of the type $U \rightarrow F \rightarrow U$ after f_1. The average dissipated work in the range $(f_1, f_{\max})$ for the U-type trajectories is given by

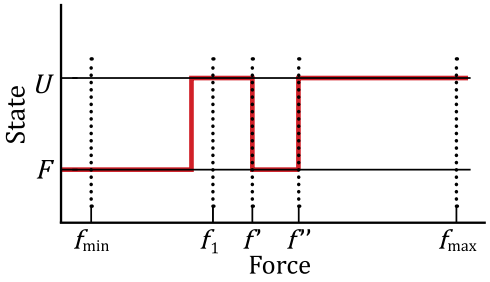

FIG. 9. Single-hopping approximation. In the model, the molecule is initially folded (F) and pulled at $\dot{f} = r_F$ and the pulling rate is changed to $\dot{f} = r_U$ at a given force value (f_1) if the molecule is observed to be unfolded (U). In the single-hopping approximation, the molecule refolds and unfolds again before $f_{\max}$. The forces that determine the trajectories $U \rightarrow F \rightarrow U$ between f_1 and $f_{\max}$ are f' and f'', which are the folding and unfolding forces, respectively.

$$\langle W_d\rangle_{U\rightarrow F\rightarrow U} = P_{U\rightarrow F\rightarrow U}(f_1)\langle f''-f'\rangle x_m, \tag{C1}$$

where x_m stands for the difference in molecular extension between U and F, f' and f'' are the folding and unfolding forces of steps $U \rightarrow F$ and $F \rightarrow U$ for the trajectory $U \rightarrow F \rightarrow U$ (Fig. 9), $P_{U\rightarrow F\rightarrow U}(f_1)$ is the fraction of trajectories of the type $U \rightarrow F \rightarrow U$, which in the current single-hopping approximation equals $1 - P^U_s(f_1, f_{\max})$ where $P^U_s(f_1, f)$ is the survival probability of U between f_1 and f. $\langle f''-f'\rangle x_m$ is given by

$$\langle f''-f'\rangle = -\int_{f_1}^{f_{\max}} df' \frac{\partial P^U_s(f_1,f')}{\partial f'} \int_{f'}^{f_{\max}} df'' P^F_s(f',f''), \tag{C2}$$

where $P^F_s(f', f'')$ is the survival probability of F between f' and f''. $\Delta\langle W_d\rangle$ is proportional to the difference of the average dissipated work between f_1 and $f_{\max}$ calculated at the pulling rates r_U and r_F. Equations (C1) and (C2) must

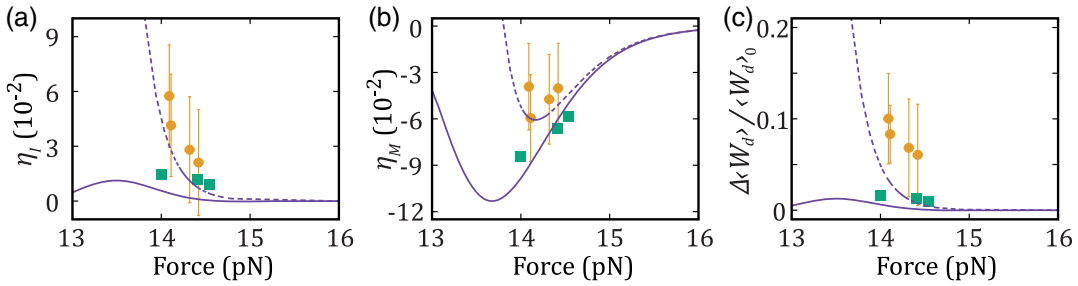

FIG. 10. The Bell-Evans model in the single-hopping approximation. (a) Dissipation-reduction efficiency η_I. (b) Information-to-measurement efficiency η_M and (c) dissipation reduction versus force from the experiments (yellow circles), simulations (green squares), the exact single-hopping approximation solution Eq. (C3) (purple line), and the $1/r$ approximation Eq. (C5) (dashed purple line).

be calculated at the pulling rates r_F and r_U to obtain the dissipation reduction in the *single-hopping* approximation,

$$\Delta\langle W_d\rangle = p^U_{\rightarrow}(r_F)[\langle W_d\rangle_{U\to F\to U}(r_U) - \langle W_d\rangle_{U\to F\to U}(r_F)], \tag{C3}$$

where $p^U_{\rightarrow}(r_F)$ is the fraction of trajectories observed at U in f_1 starting at F in $f_{\min}$, and the dissipated work is restricted to the range $(f_1, f_{\max})$. For practical purposes, we can take $f_{\max}\to\infty$ as the molecule always ends in U at $f_{\max}$. Equations (C1)–(C3) can be numerically calculated for generic Bell-Evans rates where survival probabilities have simple analytical expressions. For the specific case relevant to the experiments ($L4$ molecule) of a transition state located at half-distance between F and U, $x^\dagger = x_m/2$, we have

$$k_{F\to U}(f) = k_0 \exp(\beta f x^\dagger), \tag{C4a}$$

$$k_{F\leftarrow U}(f) = k_0 \exp[\beta(\Delta G - f x^\dagger)], \tag{C4b}$$

where k_0 is the kinetic rate at zero force, and ΔG is the free-energy difference between F and U ($\beta = 1/k_BT$). Finally, for sufficiently high forces where $k_{F\leftarrow U}(f_1)/(\beta x^\dagger r) \ll 1$, the average dissipation reduction is obtained to first order in $1/r$:

$$\Delta\langle W_d\rangle = p^U_{\rightarrow}(r_F)\left[\frac{x_m k_{F\leftarrow U}(f_1)^2}{2k_{F\to U}(f_1)(\beta x^\dagger)^2}\right]\left(\frac{1}{r_F}-\frac{1}{r_U}\right), \tag{C5}$$

which is positive for $r_U > r_F$ as expected, and negative otherwise. For practical purposes, we take $f_{\min}\to-\infty$ as the molecule always starts in F at $f_{\min}$. $p^U_{\rightarrow}(r_F)$ is expressed as

$$p^U_{\rightarrow}(r_F) = 1 - \exp\left(-\frac{k_{F\to U}(f_1)}{\beta x^\dagger r_F}\right). \tag{C6}$$

To calculate the efficiencies, we also need the values of $\langle W_d\rangle_0$ and $k_BT\Upsilon_2$ for DTF, the latter being given by Eq. (13b). $\langle W_d\rangle_0$ is estimated from the mean first unfolding force $\langle f_{F\to U}\rangle$ in the Bell-Evans approximation,

$$\begin{aligned}\langle W_d\rangle_0 &= x_m(\langle f_{F\to U}\rangle - f_c)\\ &= x_m\left[\frac{1}{\beta x^\dagger}\log\left(\frac{\beta x^\dagger r}{k_0}\right) - f_c\right],\end{aligned} \tag{C7}$$

where $f_c = \Delta G/x_m$ is the coexistence force and $k_{F\to U}(f_c) = k_{F\leftarrow U}(f_c) = k_c$ is the rate at coexistence. We also have

$$k_BT\Upsilon_2 = \log[p^F_{\leftarrow}(r_F) + p^U_{\leftarrow}(r_U)], \tag{C8a}$$

$$p^U_{\leftarrow}(r) = \exp\left(-\frac{k_{F\leftarrow U}(f)}{\beta x^\dagger r}\right), \tag{C8b}$$

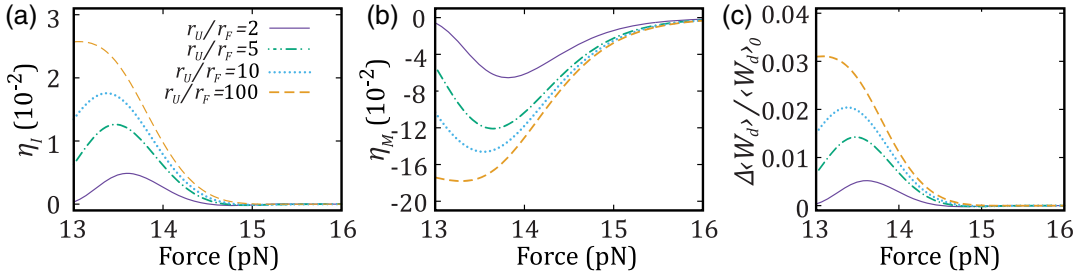

FIG. 11. Bell-Evans model prediction upon varying r_U/r_F. (a) Dissipation-reduction efficiency η_I. (b) Information-to-measurement efficiency η_M. (c) Dissipation reduction versus force using the single-hopping approximation solution.

and $p^F_{\leftarrow}(r) = 1 - p^U_{\leftarrow}(r)$. We calculate these quantities for the parameters that fit the experimental pulling curves for $L4$ without feedback ($k_0 = 2 \times 10^{-14}$ s^{-1}, $x_m = 18$ nm, $x^\dagger = 9$ nm, $k_BT = 4.114$ pN nm, $\beta = 1/k_BT \sim 0.24$ pN^{-1} nm^{-1}, $\Delta G = 264.0$ pN nm, $f_c = \Delta G x_m = 14.66$ pN, $k_c = 1.7$ s^{-1}. From these values, we calculate the efficiencies defined in Eqs. (3) and (6),

$$\eta_I = \frac{\Delta\langle W_d\rangle}{\langle W_d\rangle_0 + k_BT\Upsilon_2}, \tag{C9a}$$

$$\eta_M = \frac{\Delta\langle W_d\rangle - k_BT\Upsilon_2}{\langle W_d\rangle_0}. \tag{C9b}$$

In Fig. 10, we show η_I and η_M versus force for $r_F = 4$ pN/s and $r_U = 17$ pN/s. The purple continuous line shows the results obtained from Eqs. (C9a) and (C9b) by numerical calculation of $\Delta\langle W_d\rangle$ in the single-hopping approximation Eqs. (C1)–(C3). The dashed line shows the $1/r$ leading term Eq. (C5), which holds for sufficiently high forces [$f > 14.45$ pN where $k_{F\leftarrow U}(f)/(\beta x^\dagger r_F) \leq 0.3$]. As we can see from the figure, while η_I is small and positive (approximately 10^{-2}), η_M is small and negative (approximately -10^{-2}) in the experimentally measured range of forces. The points are the experimental results shown in Fig. 3(b).

In Fig. 11, we show the analytical Bell-Evans predictions for η_I and η_M in the single-hopping approximation for a fixed r_F and varying r_U. Interestingly, while $\Delta\langle W_d\rangle$ and η_I increase with r_U, the behavior of η_M is the opposite, becoming more negative as r_U increases.

[1] H. S. Leff and A. F. Rex, *Maxwells Demon: Entropy, Information, Computing* (Adam Hilger, Princeton, NJ, 1990), https://doi.org/10.1515/9781400861521.

[2] R. Landauer, *Irreversibility and Heat Generation in the Computing Process*, IBM J. Res. Dev. **5**, 183 (1961).

[3] C. H. Bennett, *Logical Reversibility of Computation*, IBM J. Res. Dev. **17**, 525 (1973).

[4] C. H. Bennett, *The Thermodynamics of Computation—A Review*, Int. J. Theor. Phys. **21**, 905 (1982).

[5] K. Maruyama, F. Nori, and V. Vedral, *Colloquium: The Physics of Maxwell's Demon and Information*, Rev. Mod. Phys. **81**, 1 (2009).

[6] E. Lutz and S. Ciliberto, *From Maxwell's Demon to Landauer's Eraser*, Phys. Today **68**, No. 9, 30 (2015).

[7] H. Touchette and S. Lloyd, *Information-Theoretic Limits of Control*, Phys. Rev. Lett. **84**, 1156 (2000).

[8] F. J. Cao and M. Feito, *Thermodynamics of Feedback Controlled Systems*, Phys. Rev. E **79**, 041118 (2009).

[9] T. Sagawa, *Thermodynamic and Logical Reversibilities Revisited*, J. Stat. Mech. (2014) P03025.

[10] J. M. R. Parrondo, J. M. Horowitz, and T. Sagawa, *Thermodynamics of Information*, Nat. Phys. **11**, 131 (2015).

[11] S. Toyabe, T. Sagawa, M. Ueda, E. Muneyuki, and M. Sano, *Experimental Demonstration of Information-to-Energy Conversion and Validation of the Generalized Jarzynski Equality*, Nat. Phys. **6**, 988 (2010).

[12] G. Paneru, D. Y. Lee, T. Tlusty, and H. K. Pak, *Lossless Brownian Information Engine*, Phys. Rev. Lett. **120**, 020601 (2018).

[13] G. Paneru, D. Y. Lee, J.-M. Park, J. T. Park, J. D. Noh, and H. K. Pak, *Optimal Tuning of a Brownian Information Engine Operating in a Nonequilibrium Steady State*, Phys. Rev. E **98**, 052119 (2018).

[14] T. Admon, S. Rahav, and Y. Roichman, *Experimental Realization of an Information Machine with Tunable Temporal Correlations*, Phys. Rev. Lett. **121**, 180601 (2018).

[15] J. V. Koski, V. F. Maisi, J. P. Pekola, and D. V. Averin, *Experimental Realization of a Szilard Engine with a Single Electron*, Proc. Natl. Acad. Sci. U.S.A. **111**, 13786 (2014).

[16] J. V. Koski, V. F. Maisi, T. Sagawa, and J. P. Pekola, *Experimental Observation of the Role of Mutual Information in the Nonequilibrium Dynamics of a Maxwell Demon*, Phys. Rev. Lett. **113**, 030601 (2014).

[17] M. D. Vidrighin, O. Dahlsten, M. Barbieri, M. S. Kim, V. Vedral, and I. A. Walmsley, *Photonic Maxwell's Demon*, Phys. Rev. Lett. **116**, 050401 (2016).

[18] K. Chida, S. Desai, K. Nishiguchi, and A. Fujiwara, *Power Generator Driven by Maxwell's Demon*, Nat. Commun. **8**, 15310 (2017).

[19] A. Kumar, T.-Y. Wu, F. Giraldo, and D. S. Weiss, *Sorting Ultracold Atoms in a Three-Dimensional Optical Lattice in a Realization of Maxwell's Demon*, Nature (London) **561**, 83 (2018).

[20] M. Ribezzi-Crivellari and F. Ritort, *Large Work Extraction and the Landauer Limit in a Continuous Maxwell Demon*, Nat. Phys. **15**, 660 (2019).

[21] N. Cottet, S. Jezouin, L. Bretheau, P. Campagne-Ibarcq, Q. Ficheux, J. Anders, A. Auffèves, R. Azouit, P. Rouchon, and B. Huard, *Observing a Quantum Maxwell Demon at Work*, Proc. Natl. Acad. Sci. U.S.A. **114**, 7561 (2017).

[22] Y. Masuyama, K. Funo, Y. Murashita, A. Noguchi, S. Kono, Y. Tabuchi, R. Yamazaki, M. Ueda, and Y. Nakamura, *Information-to-Work Conversion by Maxwell's Demon in a Superconducting Circuit Quantum Electrodynamical System*, Nat. Commun. **9**, 1291 (2018).

[23] M. Naghiloo, J. J. Alonso, A. Romito, E. Lutz, and K. W. Murch, *Information Gain and Loss for a Quantum Maxwell's Demon*, Phys. Rev. Lett. **121**, 030604 (2018).

[24] A. Bérut, A. Arakelyan, A. Petrosyan, S. Ciliberto, R. Dillenschneider, and E. Lutz, *Experimental Verification of Landauer's Principle Linking Information and Thermodynamics*, Nature (London) **483**, 187 (2012).

[25] A. Bérut, A. Petrosyan, and S. Ciliberto, *Detailed Jarzynski Equality Applied to a Logically Irreversible Procedure*, Europhys. Lett. **103**, 60002 (2013).

[26] Y. Jun, M. Gavrilov, and J. Bechhoefer, *High-Precision Test of Landauer's Principle in a Feedback Trap*, Phys. Rev. Lett. **113**, 190601 (2014).

[27] J. Hong, B. Lambson, S. Dhuey, and J. Bokor, *Experimental Test of Landauer's Principle in Single-Bit Operations on Nanomagnetic Memory Bits*, Sci. Adv. **2**, e1501492 (2016).

[28] J. P. S. Peterson, R. S. Sarthour, A. M. Souza, I. S. Oliveira, J. Goold, K. Modi, D. O. Soares-Pinto, and L. C. Céleri, *Experimental Demonstration of Information to Energy Conversion in a Quantum System at the Landauer Limit*, Proc. R. Soc. A **472**, 20150813 (2016).
[29] U. Seifert, *Stochastic Thermodynamics, Fluctuation Theorems and Molecular Machines*, Rep. Prog. Phys. **75**, 126001 (2012).
[30] A. Alemany, M. Ribezzi-Crivellari, and F. Ritort, *From Free Energy Measurements to Thermodynamic Inference in Nonequilibrium Small Systems*, New J. Phys. **17**, 075009 (2015).
[31] S. Ciliberto, *Experiments in Stochastic Thermodynamics: Short History and Perspectives*, Phys. Rev. X **7**, 021051 (2017).
[32] K. H. Kim and H. Qian, *Fluctuation Theorems for a Molecular Refrigerator*, Phys. Rev. E **75**, 022102 (2007).
[33] T. Sagawa and M. Ueda, *Generalized Jarzynski Equality under Nonequilibrium Feedback Control*, Phys. Rev. Lett. **104**, 090602 (2010).
[34] M. Ponmurugan, *Generalized Detailed Fluctuation Theorem under Nonequilibrium Feedback Control*, Phys. Rev. E **82**, 031129 (2010).
[35] D. Abreu and U. Seifert, *Thermodynamics of Genuine Nonequilibrium States under Feedback Control*, Phys. Rev. Lett. **108**, 030601 (2012).
[36] J. M. Horowitz and S. Vaikuntanathan, *Nonequilibrium Detailed Fluctuation Theorem for Repeated Discrete Feedback*, Phys. Rev. E **82**, 061120 (2010).
[37] T. Sagawa and M. Ueda, *Nonequilibrium Thermodynamics of Feedback Control*, Phys. Rev. E **85**, 021104 (2012).
[38] Y. Ashida, K. Funo, Y. Murashita, and M. Ueda, *General Achievable Bound of Extractable Work under Feedback Control*, Phys. Rev. E **90**, 052125 (2014).
[39] S. Lahiri and A. M. Jayannavar, *Extended Fluctuation Theorems for Repeated Measurements and Feedback within Hamiltonian Framework*, Phys. Lett. A **380**, 1706 (2016).
[40] D. Mandal and C. Jarzynski, *Work and Information Processing in a Solvable Model of Maxwell's Demon*, Proc. Natl. Acad. Sci. U.S.A. **109**, 11641 (2012).
[41] P. Strasberg, G. Schaller, T. Brandes, and M. Esposito, *Thermodynamics of a Physical Model Implementing a Maxwell Demon*, Phys. Rev. Lett. **110**, 040601 (2013).
[42] R. Sánchez, P. Samuelsson, and P. P. Potts, *Autonomous Conversion of Information to Work in Quantum Dots*, Phys. Rev. Research **1**, 033066 (2019).
[43] B. Annby-Andersson, P. Samuelsson, V. F. Maisi, and P. P. Potts, *Maxwell's Demon in a Double Quantum Dot with Continuous Charge Detection*, Phys. Rev. B **101**, 165404 (2020).
[44] J. M. Horowitz and J. M. R. Parrondo, *Designing Optimal Discrete-Feedback Thermodynamic Engines*, New J. Phys. **13**, 123019 (2011).
[45] J. Bechhoefer, *Feedback for Physicists: A Tutorial Essay on Control*, Rev. Mod. Phys. **77**, 783 (2005).
[46] E. Dieterich, J. Camunas-Soler, M. Ribezzi-Crivellari, U. Seifert, and F. Ritort, *Control of Force through Feedback in Small Driven Systems*, Phys. Rev. E **94**, 012107 (2016).
[47] G. Verley, M. Esposito, T. Willaert, and C. Van den Broeck, *The Unlikely Carnot Efficiency*, Nat. Commun. **5**, 4721 (2014).
[48] R. K. Schmitt, J. M. R. Parrondo, H. Linke, and J. Johansson, *Molecular Motor Efficiency is Maximized in the Presence of Both Power-Stroke and Rectification through Feedback*, New J. Phys. **17**, 065011 (2015).
[49] M. Ribezzi-Crivellari and F. Ritort, *Work Extraction, Information-Content and the Landauer Bound in the Continuous Maxwell Demon*, J. Stat. Mech. (2019) 084013.
[50] I. Junier, A. Mossa, M. Manosas, and F. Ritort, *Recovery of Free Energy Branches in Single Molecule Experiments*, Phys. Rev. Lett. **102**, 070602 (2009).
[51] A. Alemany, A. Mossa, I. Junier, and F. Ritort, *Experimental Free-Energy Measurements of Kinetic Molecular States Using Fluctuation Theorems*, Nat. Phys. **8**, 688 (2012).
[52] J. Camunas-Soler, A. Alemany, and F. Ritort, *Experimental Measurement of Binding Energy, Selectivity, and Allostery Using Fluctuation Theorems*, Science **355**, 412 (2017).
[53] M. Palassini and F. Ritort, *Improving Free-Energy Estimates from Unidirectional Work Measurements: Theory and Experiment*, Phys. Rev. Lett. **107**, 060601 (2011).
[54] J. M. Huguet, C. V. Bizarro, N. Forns, S. B. Smith, C. Bustamante, and F. Ritort, *Single-Molecule Derivation of Salt Dependent Base-Pair Free Energies in DNA*, Proc. Natl. Acad. Sci. U.S.A. **107**, 15431 (2010).
[55] N. Forns, S. de Lorenzo, M. Manosas, K. Hayashi, J. M. Huguet, and F. Ritort, *Improving Signal/Noise Resolution in Single-Molecule Experiments Using Molecular Constructs with Short Handles*, Biophys. J. **100**, 1765 (2011).
[56] G. E. Crooks, *Entropy Production Fluctuation Theorem and the Nonequilibrium Work Relation for Free Energy Differences*, Phys. Rev. E **60**, 2721 (1999).
[57] See Supplemental Material at http://link.aps.org/supplemental/10.1103/PhysRevX.11.031052 for complementary and supporting results.
[58] É. Roldán, I. A. Martinez, J. M. R. Parrondo, and D. Petrov, *Universal Features in the Energetics of Symmetry Breaking*, Nat. Phys. **10**, 457 (2014).
[59] J. M. Horowitz and H. Sandberg, *Second-Law-Like Inequalities with Information and Their Interpretations*, New J. Phys. **16**, 125007 (2014).
[60] I. J. Ford, *Maxwell's Demon and the Management of Ignorance in Stochastic Thermodynamics*, Contemp. Phys. **57**, 309 (2016).
[61] M. Gavrilov, R. Chétrite, and J. Bechhoefer, *Direct Measurement of Weakly Nonequilibrium System Entropy is Consistent with Gibbs-Shannon Form*, Proc. Natl. Acad. Sci. U.S.A. **114**, 11097 (2017).
[62] R. Alicki and M. Horodecki, *Information-Thermodynamics Link Revisited*, J. Phys. A **52**, 204001 (2019).
[63] S. Tafoya, S. J. Large, S. Liu, C. Bustamante, and D. A. Sivak, *Using a Systems Equilibrium Behavior to Reduce Its Energy Dissipation in Nonequilibrium Processes*, Proc. Natl. Acad. Sci. U.S.A. **116**, 5920 (2019).
[64] M. Poot and H. S. van der Zant, *Mechanical Systems in the Quantum Regime*, Phys. Rep. **511**, 273 (2012).
[65] S. Sheikhfaal, S. Angizi, S. Sarmadi, M. H. Moaiyeri, and S. Sayedsalehi, *Designing Efficient QCA Logical Circuits with Power Dissipation Analysis*, Microelectron. J. **46**, 462 (2015).
[66] H. Ozawa, A. Ohmura, R. D. Lorenz, and T. Pujol, *The Second Law of Thermodynamics and the Global Climate*

System: A Review of the Maximum Entropy Production Principle, Rev. Geophys. **41**, 1 (2003).

[67] C. W. Wächtler, P. Strasberg, and T. Brandes, *Stochastic Thermodynamics Based on Incomplete Information: Generalized Jarzynski Equality with Measurement Errors with or without Feedback*, New J. Phys. **18**, 113042 (2016).

[68] P. P. Potts and P. Samuelsson, *Detailed Fluctuation Relation for Arbitrary Measurement and Feedback Schemes*, Phys. Rev. Lett. **121**, 210603 (2018).

[69] T. Munakata and M. L. Rosinberg, *Entropy Production and Fluctuation Theorems for Langevin Processes under Continuous Non-Markovian Feedback Control*, Phys. Rev. Lett. **112**, 180601 (2014).

[70] M. Debiossac, D. Grass, J. J. Alonso, E. Lutz, and N. Kiesel, *Thermodynamics of Continuous Non-Markovian Feedback Control*, Nat. Commun. **11**, 1360 (2020).

[71] S. Ito and T. Sagawa, *Maxwell's Demon in Biochemical Signal Transduction with Feedback Loop*, Nat. Commun. **6**, 7498 (2015).

[72] R. A. Brittain, N. S. Jones, and T. E. Ouldridge, *Biochemical Szilard Engines for Memory-Limited Inference*, New J. Phys. **21**, 063022 (2019).

[73] E. Tang and R. Golestanian, *Quantifying Configurational Information for a Stochastic Particle in a Flow-Field*, New J. Phys. **22**, 083060 (2020).

[74] L. Dabelow, S. Bo, and R. Eichhorn, *Irreversibility in Active Matter Systems: Fluctuation Theorem and Mutual Information*, Phys. Rev. X **9**, 021009 (2019).

[75] T. Sagawa and M. Ueda, *Fluctuation Theorem with Information Exchange: Role of Correlations in Stochastic Thermodynamics*, Phys. Rev. Lett. **109**, 180602 (2012).

[76] J. V. Koski, A. Kutvonen, I. M. Khaymovich, T. Ala-Nissila, and J. P. Pekola, *On-Chip Maxwell's Demon as an Information-Powered Refrigerator*, Phys. Rev. Lett. **115**, 260602 (2015).

[77] A. Mossa, M. Manosas, N. Forns, J. M. Huguet, and F. Ritort, *Dynamic Force Spectroscopy of DNA Hairpins: I. Force Kinetics and Free Energy Landscapes*, J. Stat. Mech. (2009) P02060.